mat LB9507 luminometer. We thank members of Division of Molecular Pathology for constructive criticism and fruitful discussion. This work was supported in part by a Grant-in-Aid for Young Scientists (B) [24790310 for M.SY.] and a Grant-in-Aid for Scientific Research (B) [22300336 for Y.M.] from the Ministry of Education, Culture, Sports, Science, and Technology, Japan; a Grant-in-Aid for the Third Term Comprehensive Control Research for Cancer from the Ministry of Health, Labor, and Welfare, Japan [Y.M.]; and a Grant from the Smoking Research Foundation, Japan [Y.M.].

REFERENCES

[1] M. Kuramochi, H. Fukuhara, T. Nobukuni, T. Kanbe, T. Maruyama, H. P. Ghosh, M. Pletcher, M. Isomura, M. Onizuka, T. Kitamura, T. Sekiya, R. H. Reeves, Y. Murakami, "TSLC1 is a tumor-suppressor gene in human non-small-cell lung cancer," *Nature Genetics*, Vol. 27, No. 4, 2001, pp. 427-430.

[2] M. Masuda, M. Yageta, H. Fukuhara, M. Kuramochi, T. Maruyama, A. Nomoto, Y. Murakami, "The tumor suppressor protein TSLC1 is involved in cell-cell adhesion," *J Biological Chemistry*, Vol. 277, No. 34, 2002, pp. 31014-31019.

[3] T. Fukami, H. Fukuhara, M. Kuramochi, T. Maruyama, K. Isogai, M. Sakamoto, S. Takamoto, Y. Murakami, "Promoter methylation of the TSLC1 gene in advanced lung tumors and various cancer cell lines," *International Journal of Cancer*, Vol. 107, No. 1, 2003, pp. 53-59. doi:10.1002/ijc.11348

[4] K. Uchino, A. Ito, T. Wakayama, Y. Koma, T. Okada, C. Ohbayashi, S. Iseki, Y. Kitamura, N. Tsubota, Y. Okita, M. Okada, "Clinical implication and prognostic significance of the tumor suppressor TSLC1 gene detected in adenocarcinoma of the lung," *Cancer*, Vol. 98, No. 5, 2003, pp. 1002-1007. doi:10.1002/cncr.11599

[5] A. Goto, T. Niki, L. Chi-Pin, D. Matsubara, Y. Murakami, N. Funata, M. Fukayama, "Loss of TSLC1 expression in lung adenocarcinoma: relationships with histological subtypes, sex and prognostic significance," *Cancer Science*, Vol. 96, No. 8, 2005, pp. 480-486. doi:10.1111/j.1349-7006.2005.00075.x

[6] W. Zhang, L. Zhou, S. M. Ding, H. Y. Xie, X. Xu, J. Wu, Q. X. Chen, F. Zhang, B. J. Wei, A. T. Eldin, S. S. Zheng, "Aberrant methylation of the CADM1 promoter is associated with poor prognosis in hepatocellular carcinoma treated with liver transplantation," *Oncology Reports*, Vol. 25, No. 4, 2011, pp. 1053-1062. doi:10.3892/or.2011.1159

[7] T. Ito, Y. Shimada, Y. Hashimoto, J. Kaganoi, T. Kan, G. Watanabe, Y. Murakami, M. Imamura, "Involvement of TSLC1 in progression of esophageal squamous cell carcinoma," *Cancer Research*, Vol. 63, No. 19, 2003, pp. 6320-6326.

[8] Y. Murakami, "Involvement of a cell adhesion molecule, TSLC1/IGSF4, in human oncogenesis," *Cancer Science*, Vol. 96, No. 9, 2005, pp. 543-552. doi: 10.1111/j.1349-7006.2005.00089.x

[9] D. P. Bartel, "MicroRNAs: genomics, biogenesis, mechanism, and function," *Cell*, Vol. 116, No. 2, 2004, pp. 281-297.

[10] M. Seike, A. Goto, T. Okano, E. D. Bowman, A. J. Schetter, I. Horikawa, E. A. Mathe, J. Jen, P. Yang, H. Sugimura, A. Gemma, S. Kudoh, C. M. Croce, C. C. Harris, "MiR-21 is an EGFR-regulated anti-apoptotic factor in lung cancer in never-smokers," *Proceedings of the National Academy of Science of the United States of America*, Vol. 106, No. 29, 2009, pp. 12085-12090. doi:10.1073/pnas.0905234106

[11] F. Talotta, A. Cimmino, M. R. Matarazzo, L. Casalino, G. De Vita, M. D'Esposito, R. Di Lauro, P. Verde, "An autoregulatory loop mediated by miR-21 and PDCD4 controls the AP-1 activity in RAS transformation," *Oncogene*, Vol. 28, No. 1, 2009, pp.73-84. doi:10.1038/onc.2008.370

[12] S. M. Johnson, H. Grosshans, J. Shingara, M. Byrom, R. Jarvis, A. Cheng, E. Labourier, K. L. Reinert, D. Brown, F. J. Slack, "RAS is regulated by the let-7 microRNA family," *Cell*, Vol. 120, No. 5, 2005, pp.635-647. doi:10.1016/j.cell.2005.01.014

[13] T. Ito, Y. Williams-Nate, M. Iwai, Y. Tsuboi, M. Hagiyama, A. Ito, M. Sakurai-Yageta, Y. Murakami, "Transcriptional regulation of the CADM1 gene by retinoic acid during the neural differentiation of murine embryonal carcinoma P19 cells," *Genes to Cells*, Vol. 16, No. 7, 2011, pp. 791-802. doi:10.1111/j.1365-2443.2011.01525.x

[14] J. G. Herman, J. R. Graff, S. Myohanen, B. D. Nelkin, S. B. Baylin, "Methylation-specific PCR: a novel PCR assay for methylation status of CpG islands," *Proceedings of the National Academy of Science of the United States of America*, Vol. 93, No. 18, 1996, pp.9821-9826.

[15] B. P. Lewis, I. H. Shih, M. W. Jones-Rhoades, D. P. Bartel, C. B. Burge, "Prediction of mammalian microRNA targets," *Cell*, Vol. 115, No.7, 2003, pp. 787-798.

[16] A. Krek, D. Grun, M. N. Poy, R. Wolf, L. Rosenberg, E. J. Epstein, P. MacMenamin, I. da Piedade, K. C. Gunsalus, M. Stoffel, N. Rajewsky, "Combinatorial microRNA target predictions," *Nature Genetics*,

Vol. 37, No. 5, 2005, pp. 495-500. doi:10.1038/ng1536

[17] S. Kikuchi, D. Yamada, T. Fukami, T. Maruyama, A. Ito, H. Asamura, Y. Matsuno, M. Onizuka, Y. Murakami. "Hypermethylation of the TSLC1/IGSF4 promoter is associated with tobacco smoking and a poor prognosis in primary non-small cell lung cancer," *Cancer*, Vol. 106, No. 8, 2006, pp1751-1758. doi:10.1002/cncr.21800

[18] X. Mao, E. Seidlitz, K. Ghosh, Y. Murakami, H. P. Ghosh, "The cytoplasmic domain is critical to the tumor suppressor activity of TSLC1 in non-small cell lung cancer," *Cancer Research*, Vol. 63, No. 22, 2003, pp.7979-7985.

[19] M. N. Poy, J. Hausser, M. Trajkovski, M. Braun, S. Collins, P. Rorsman, M. Zavolan, M. Stoffel, "miR-375 maintains normal pancreatic alpha- and beta-cell mass," *Proceedings of the National Academy of Science of the United States of America*, Vol. 106, No. 14, 2009, pp.5813-5818. doi:10.1073/pnas.0810550106

[20] H. Yang, W. Kong, L. He, J. J. Zhao, J. D. O'Donnell, J. Wang, R. M. Wenham, D. Coppola, P. A. Kruk, S. V. Nicosia, J. Q. Cheng, "MicroRNA expression profiling in human ovarian cancer: miR-214 induces cell survival and cisplatin resistance by targeting PTEN," *Cancer Research*, Vol. 68, No. 2, 2008, pp. 425-433. doi:10.1158/0008-5472.CAN-07-2488

[21] G. Yin, R. Chen, A. B. Alvero, H. H. Fu, J. Holmberg, C. Glackin, T. Rutherford, G. Mor, "TWISTing stemness, inflammation and proliferation of epithelial ovarian cancer cells through MIR199A2/214," *Oncogene*, Vol. 29, No. 24, 2010, pp.3545-3553. doi:10.1038/onc.2010.111

[22] E. Penna, F. Orso, D. Cimino, E. Tenaglia, A. Lembo, E. Quaglino, L. Poliseno, A. Haimovic, S. Osella-Abate, C. De Pitta, E. Pinatel, M. B. Stadler, P. Provero, M. G. Bernengo, I. Osman, D. Taverna, "microRNA-214 contributes to melanoma tumour progression through suppression of TFAP2C," *EMBO Journal*, Vol. 30, No.10, 2011, pp.1990-2007. doi:10.1038/emboj.2011.102

[23] P. de Souza Rocha Simonini, A. Breiling, N. Gupta, M. Malekpour, M. Youns, R. Omranipour, F. Malekpour, S. Volinia, C. M. Croce, H. Najmabadi, S. Diederichs, O. Sahin, D. Mayer, F. Lyko, J. D. Hoheisel, Y. Riazalhosseini, "Epigenetically deregulated microRNA-375 is involved in a positive feedback loop with estrogen receptor alpha in breast cancer cells," *Cancer Research*, Vol. 70, No. 22, 2010, pp.9175-9184. doi:10.1158/0008-5472.CAN-10-1318

[24] Y. Tsukamoto, C. Nakada, T. Noguchi, M. Tanigawa, L. T. Nguyen, T. Uchida, N. Hijiya, K. Matsuura, T. Fujioka, M. Seto, M. Moriyama, "MicroRNA-375 is downregulated in gastric carcinomas and regulates cell survival by targeting PDK1 and 14-3-3zeta," *Cancer Research*, Vol. 70, No. 6, 2010, pp.2339-2349. doi:10.1158/0008-5472.CAN-09-2777

[25] L. Ding, Y. Xu, W. Zhang, Y. Deng, M. Si, Y. Du, H. Yao, X. Liu, Y. Ke, J. Si, T. Zhou, "MiR-375 frequently downregulated in gastric cancer inhibits cell proliferation by targeting JAK2," *Cell Research*, Vol. 20, No.7, 2010, pp. 784-793. doi: 10.1038/cr.2010.79

[26] E. A. Mathe, G. H. Nguyen, E. D. Bowman, Y. Zhao, A. Budhu, A. J. Schetter, R. Braun, M. Reimers, K. Kumamoto, D. Hughes, N. K. Altorki, A. G. Casson, C. G. Liu, X. W. Wang, N. Yanaihara, N. Hagiwara, A. J. Dannenberg, M. Miyashita, C. M. Croce, C. C. Harris, "MicroRNA expression in squamous cell carcinoma and adenocarcinoma of the esophagus: associations with survival," *Clinical Cancer Research*, Vol. 15, No. 19, 2009, pp.6192-6200. doi:10.1158/1078-0432.CCR-09-1467

[27] L. Yu, N. W. Todd, L. Xing, Y. Xie, H. Zhang, Z. Liu, H. Fang, J. Zhang, R. L. Katz, F. Jiang, "Early detection of lung adenocarcinoma in sputum by a panel of microRNA markers," *International Journal of Cancer*, Vol. 127, No. 12, 2010, pp.2870-2878. doi:10.1002/ijc.25289

Cancer Science
The official journal of the Japanese Cancer Association JCA

Lung cancer with loss of BRG1/BRM, shows epithelial mesenchymal transition phenotype and distinct histologic and genetic features

Daisuke Matsubara,[1,2] Yuka Kishaba,[1] Shumpei Ishikawa,[3] Takashi Sakatani,[1] Sachiko Oguni,[1] Tomoko Tamura,[1] Hiroko Hoshino,[1] Yukihiko Sugiyama,[4] Shunsuke Endo,[5] Yoshinori Murakami,[2] Hiroyuki Aburatani,[6] Masashi Fukayama[3] and Toshiro Niki[1,7]

[1]Department of Integrative Pathology, Jichi Medical University, Shimotsuke, Tochigi; [2]Division of Molecular Pathology, Institute of Medical Science, The University of Tokyo, Minato-ku, Tokyo; [3]Department of Human Pathology, Graduate School of Medicine, The University of Tokyo, Bunkyo-ku, Tokyo; [4]Division of Pulmonary Medicine, Jichi Medical University, Tochigi; [5]Division of General Thoracic Surgery, Jichi Medical University, Shimotsuke, Tochigi; [6]Division of Genome Science, Research Center for Advanced Science and Technology, The University of Tokyo, Meguro-ku, Tokyo, Japan

(Received August 22, 2012/Revised October 30, 2012/Accepted November 6, 2012/Accepted manuscript online November 19, 2012/Article first published online January 4, 2013)

BRG1 and BRM, two core catalytic subunits in SWI/SNF chromatin remodeling complexes, have been suggested as tumor suppressors, yet their roles in carcinogenesis are unclear. Here, we present evidence that loss of BRG1 and BRM is involved in the progression of lung adenocarcinomas. Analysis of 15 lung cancer cell lines indicated that BRG1 mutations correlated with loss of BRG1 expression and that loss of BRG1 and BRM expression was frequent in E-cadherin-low and vimentin-high cell lines. Immunohistochemical analysis of 93 primary lung adenocarcinomas showed loss of BRG1 and BRM in 11 (12%) and 16 (17%) cases, respectively. Loss of expression of BRG1 and BRM was frequent in solid predominant adenocarcinomas and tumors with low thyroid transcription factor-1 (TTF-1, master regulator of lung) and low cytokeratin7 and E-cadherin (two markers for bronchial epithelial differentiation). Loss of BRG1 was correlated with the absence of lepidic growth patterns and was mutually exclusive of epidermal growth factor receptor (EGFR) mutations. In contrast, loss of BRM was found concomitant with lepidic growth patterns and EGFR mutations. Finally, we analyzed the publicly available dataset of 442 cases and found that loss of BRG1 and BRM was frequent in E-cadherin-low, TTF-1-low, and vimentin-high cases and correlated with poor prognosis. We conclude that loss of either or both BRG1 and BRM is involved in the progression of lung adenocarcinoma into solid predominant tumors with features of epithelial mesenchymal transition and loss of the bronchial epithelial phenotype. BRG1 loss was specifically involved in the progression of EGFR wild-type, but not EGFR-mutant tumors. (*Cancer Sci* 2013; 104: 266–273)

Lung cancer is the leading cause of cancer death in many developed countries, including the United States and Japan.[1,2] The identification of genetic abnormalities, such as epidermal growth factor receptor (EGFR) mutations, KRAS mutations, EML4–ALK translocation, and MET amplifications has revolutionized our understanding of the molecular mechanisms in lung cancer development.[3] However, it has become increasingly apparent that epigenetic alternations play equally important roles in tumorigenesis, and among them, chromatin remodeling factors have attracted much attention recently.[4] Indeed, identification of mutations of chromatin remodeling factors in cancer has been a major hot topic in the past 2 years.[5–8]

BRG1 and BRM, two core catalytic ATPase subunits in human SWI/SNF chromatin remodeling enzymes, have now emerged as bona fide tumor suppressor genes.[9–12] Inactivating mutations of BRG1 have been identified in 35% of non-small cell lung cancer cell lines and a subset of primary lung cancer.[9] In a mouse model of lung cancer, targeted knockout of BRG1 can affect tumor development.[10] In contrast to BRG1, mutations of BRM have rarely been identified and epigenetic silencing of BRM plays a contributory role in some cancers.[4,11] However, whether loss of BRG1 and BRM affects phenotype and differentiation of lung cancer cells remains unexplored. Furthermore, the previous studies were conducted before the discovery of EGFR mutations, and thus relationship between the EGFR status and loss of BRG1 and BRM is completely unknown.

We have recently demonstrated that lung adenocarcinoma could be classified into two groups based on the patterns of gene expression and genetic abnormalities; bronchial epithelial phenotype tumors and mesenchymal-like phenotype tumors.[13] "Bronchial epithelial phenotype" represents a group of lung adenocarcinomas with high expression of bronchial epithelial markers. This group includes thyroid transcription factor (TTF)-1 positive terminal respiratory unit (TRU) type[14] in addition to TTF-1 negative tumors with high expression of bronchial epithelial markers such as CK7 and MUC1, as detailed in our previous report.[13] Bronchial epithelial phenotype tumor exhibits high phosphorylation of EGFR and MET and frequent mutations or amplifications of EGFR, MET, and HER2. In contrast, mesenchymal-like phenotype tumors were characterized by the absence of the bronchial epithelial phenotype, triple-negative for TTF-1, MUC1, and CK7, showed no or little phosphorylation of EGFR and MET, no mutation or amplification of EGFR, MET, or HER2, and with features of epithelial mesenchymal transition (EMT), such as low E-cadherin and high FGFR1, vimentin, and ZEB1 expressions.[13] The absence of mutations or amplifications of EGFR, MET, or HER2 in mesenchymal-like phenotype tumors suggested to us that other genetic or epigenetic abnormalities may play a role in this group of tumors.

We now show in this paper that loss of expression of chromatin remodeling factors, BRG1 and BRM, correlated with features of mesenchymal-like phenotype with solid predominant histology. In particular, BRG1 loss occurred exclusively in EGFR wild-type tumors.

[7]To whom correspondence should be addressed.
E-mail: tniki@jichi.ac.jp

doi: 10.1111/cas.12065

Materials and Methods

Cell lines and medium. We used 19 non-small cell lung cancer (NSCLC) cell lines; 15 adenocarcinoma cell lines (H23, H358, H441, H522, H1395, H1648, H1650, H1703, H1795, H2087, HCC827, HCC4006, Calu3, A549, PC-3), three large cell carcinoma cell lines (H661, H1299, Lu65), and one adenosquamous cell line (H596). HCC827, H1650, H1975, PC-3, and HCC4006 were EGFR-mutated cell lines. The sources of the cell lines were described in our previous report.[13] All cell lines were maintained in RPMI1640 supplemented with 10% FCS, glutamine, and antibiotics in a humidified atmosphere with 5% CO_2 and 95% air.

Genetic and protein analysis of cell lines. The DNA, RNA, and cell lysates were prepared from cell lines by standard procedures. Experimental details of sequencing, copy number analyses, and Western blotting are given in Doc. S1. Antibodies used in western blot analysis were summarized in Table 1.

Patients and tumors. Tumor specimens were obtained from 93 patients who underwent lung cancer surgery at the Jichi medical university hospital during the period from October 2005 to June 2008. The demographic and clinicopathologic details of the patients and tumors are provided in Doc. S1.

Immunohistochemistry and evaluation. Formalin-fixed, paraffin-embedded tumor specimens were analyzed by immunohistochemistry using antibodies to BRG1, BRM, E-cadherin, cytokeratin 7, MUC1, TTF-1, p-EGF, and p-MET. The sources of antibodies, staining procedures, and methods of evaluation, are given in Doc. S1.

Mutation analyses of formalin-fixed, paraffin-embedded tissue sections. Details are shown in Doc. S1.

Bioinformatic analyses and statistics. Details are shown in Doc. S1.

Results

Characteristics of lung adenocarcinoma cell lines with loss of BRG1 and/or BRM. First, we used 15 lung cancer cell lines, for which the mutational status of BRG1 was known, to investigate the molecular features that may characterize lung adenocarcinoma cell lines with loss of BRG1. Of the 15 cell lines, six cell lines harbored BRG1 mutations and nine cell lines did not, according to previous literature,[9,11] and the Sanger COSMIC database (http://www.sanger.ac.uk/genetics/CGP/cosmic/).

Figure 1 summarizes (i) the genetic status of BRG1, EGFR, MET, HER2, BRAF, and KRAS (upper panel), (ii) gene level expressions of BRG1, BRM, TTF1, MUC1, CK7, E-cadherin, and vimentin (middle panel), and (iii) protein expression levels of BRG1, BRM, TTF1, MUC1, CK7, E-cadherin, and vimentin (lower panel) of the 15 cell lines (the microarray analysis data of 15 cell lines is located in Data S1). All six BRG1-mutated cell lines showed extreme loss of BRG1 at gene and protein levels, EMT features (low E-cadherin and high vimentin), and loss of bronchial epithelial markers (TTF-1, CK7, and MUC1). In contrast, the nine BRG1-wild type cell lines showed high expressions of BRG1, as well as high expressions of bronchial epithelial markers and E-cadherin and low expression of vimentin, at both gene and protein levels. As for gene abnormalities, BRG1-wild type cell lines showed gene abnormalities for EGFR, MET, HER2, BRAF, or KRAS, but BRG1 mutated cell lines showed no such genetic abnormalities, except for KRAS mutations.

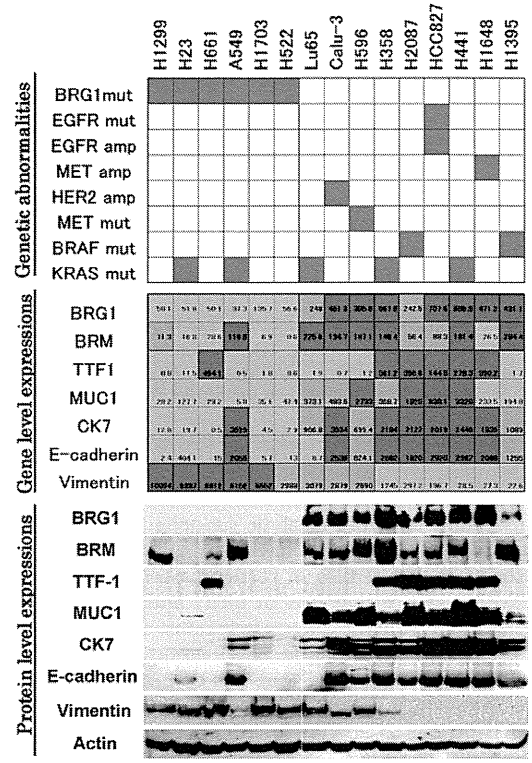

Fig. 1. Genetic status of BRG1, epidermal growth factor receptor (EGFR), MET, HER2, BRAF, and KRAS (upper panel), gene level expressions of BRG1, BRM, TTF1, MUC1, CK7, E-cadherin, and vimentin (middle panel), and protein expression levels of BRG1, BRM, TTF1, MUC1, CK7, E-cadherin, and vimentin (lower panel) of the 15 cell lines. In the upper panel, the grey box means presence of genetic abnormalities and the white box means absence of genetic abnormalities. Color indications in the middle lane are as follows: red means more than or equal to the average of each gene expression; orange: under the average and more than or equal to half the average; and green: under half the average.

We also examined the expressions of BRM in the same cell lines. Of the 15 cell lines, 10 cell lines expressed the BRM protein at modest or high levels, which was largely concordant

Table 1. Antibodies used in western blot analysis

Antibodies	Clone	Sources
BRG1 (sc-17796)	Mouse monoclonal	Santa Cruz Biotechnology (Santa Cruz, CA, USA)
BRM (A301-016A)	Rabbit polyclonal	Bethyl Laboratory (Montgomery, TX, USA)
TTF-1 (clone 8G7G3/1)	Mouse monoclonal	DAKO (Glostrup, Denmark)
Cytokeratin 7 (clone OV-TL 12/30)	Mouse monoclonal	DAKO (Glostrup, Denmark)
Vimentin (clon V9)	Mouse monoclonal	DAKO (Glostrup, Denmark)
E-cadherin (clone 36)	Mouse monoclonal	BD Biosciences (Franklin Lakes, NJ, USA)
MUC1 smaller cytoplasmic subunit	Hamster monoclonal	Lab Vision (Cheshire, UK)
Anti-rabbit IgG peroxidase conjugate		Amersham (Arlington Hights, IL, USA)
Anti-mouse IgG peroxidase conjugate		Amersham (Arlington Hights, IL, USA)
Anti-Armenian hamster IgG peroxidase conjugate		Jackson Immunoresearch (West Grove, PA, USA)

with gene expression (Fig. 1). As with BRG1, loss of BRM expression was similarly frequent in cell lines with EMT features and loss of the bronchial epithelial phenotype.

These results suggest the following: (i) loss of either or both BRG1 and BRM would be involved in the acquisition of EMT features and loss of the bronchial phenotype; and (ii) loss of BRG1 gene and protein expression correlate with the BRG1 mutation status.

We conducted the same analysis in five EGFR-mutated cell lines (HCC827, H1650, H1975, PC-3, and HCC4006), as shown in Figure S1. Although genetic status of BRG1 was unknown in H1650, H1975, PC-3, and HCC4006, all five EGFR-mutated cell lines showed high expression levels of BRG1, which suggested that loss of BRG1 would be mutually exclusive with EGFR mutations.

Immunohistochemical expression of BRG1 and BRM in primary lung adenocarcinoma tissues. Next, we used 93 cases of primary lung adenocarcinoma cases in our institution to examine the immunohistochemical expressions of BRG1 and BRM and their relationship with (i) histopathological subtypes, (ii) presence or absence of lepidic growth components, (iii) expressions of E-cadherin, TTF-1, CK7, and MUC1, (iv) genetic status of EGFR and KRAS, and (v) activation levels of EGFR and MET.

Overall, in the large majority of cases (>80%), nuclear staining for BRG1 and BRM was observed in cancer cells (Figs 2,3). Stromal cells constantly stained positive for BRG1 and BRM, and thus served as excellent internal positive controls. Using the criteria described in the Methods (Doc. S1), 11 cases (12%) were judged as showing low expression levels of BRG1 and 16 cases (17%) as showing low expression levels of BRM. Five cases (5%) showed low expression levels of both BRG1 and BRM. Most of the BRG1-low cases were either completely negative or showed only scattered positive staining for BRG1. In contrast, BRM showed a more heterogeneous staining pattern, typically showing strong positive staining in lepidic growth components, while showing negative or weak staining in invasive high-grade components (Fig. 4A–C).

Table 2 shows correlations between the expression levels of BRG1 and BRM and histopathological subtypes. All cases of well differentiated adenocarcinomas, that is, adenocarcinoma *in situ* (AIS) and minimally invasive adenocarcinoma (MIA), showed positive immunostaining for both BRG1 and BRM (20 of 20, 100%; Figs 2A,3A). Moderately differentiated adenocarcinomas, that is, acinar or papillary adenocarcinoma, also frequently showed positive immunostaining for both BRG1 and BRM (37 of 46, 80%; Figs 2B,3B), while some of them showed loss of either BRG1 or BRM (9 of 46, 20%; Figs 2D,3D). In contrast to these well- to moderately-differentiated tumors, poorly-differentiated adenocarcinomas (solid adenocarcinomas) frequently showed loss of expression of either BRG1 or BRM (12 of 13, 92%; Figs 2C,3C). Most cases (4 of 5, 80%) with loss of both BRG1 and BRM showed solid morphology (Table 2). One of three cases (33%) of invasive mucinous adenocarcinoma showed loss of BRG1.

We also examined correlations between the expression levels of BRG1 and BRM and the presence or absence of lepidic growth components (Table 3). Strikingly, all cases with BRG1 loss were devoid of lepidic growth components, while 6 of 16 cases with BRM loss showed lepidic growth components (Table 3).

Table 4 shows correlations between the expression levels of BRG1 and BRM and that of bronchial epithelial markers (TTF-1, CK7, and, MUC1) and E-cadherin. The expressions of TTF-1, CK7, MUC1 (membranous expression), and E-cadherin were frequently reduced in cases with loss of BRG1 and BRM (shown in Fig. S2). In particular, loss of E-cadherin and TTF-1 was remarkably correlated with loss of BRG1; all but one case of E-cadherin-low tumors showed BRG1 loss and all cases with BRG1 loss showed low expression levels of TTF-1. Depolarized expression of MUC1 was also frequent in cases with loss of BRG1 and BRM.

Table 4 also shows correlations between the expression levels of BRG1 and BRM and genetic status of EGFR and KRAS. Mutually exclusive correlations were observed between EGFR mutations and BRG1 loss ($P = 0.0006$), but no significant correlations between EGFR mutations and BRM loss ($P = 0.3382$). KRAS mutations were sometimes harbored by cases with loss of BRG1 or BRM.

We also examined the expressions of phospho-EGFR and phospho-MET and compared them with the expressions of BRG1 and BRM (Table 4). Low phosphorylation levels of EGFR were significantly correlated with loss of BRG1 and BRM ($P = 0.0003$, $P < 0.0001$, respectively). Phosphorylation

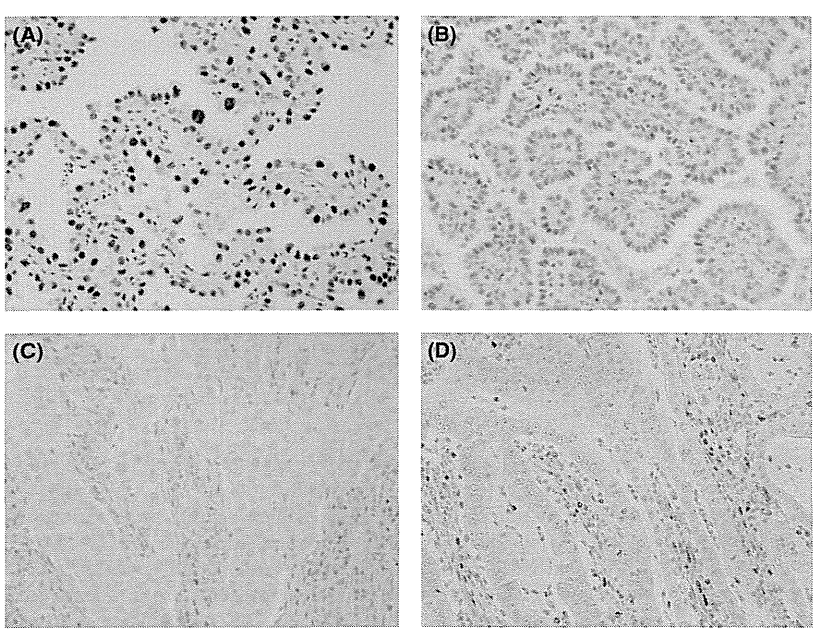

Fig. 2. BRG1 expressions in lung adenocarcinomas. Overall, more than 80% of cases showed positivity for BRG1. (A) Lepidic growth components showed strong immunoreactivity for BRG1. (B) Moderately differentiated adenocarcinomas, such as papillary adenocarcinoma, frequently showed positivity for BRG1. (C) Solid adenocarcinomas with mucin were frequently negatively stained for BRG1. (D) Some cases with papillary or acinar morphology showed negative staining for BRG1. Note BRG1 positivity in stromal cells.

doi: 10.1111/cas.12065

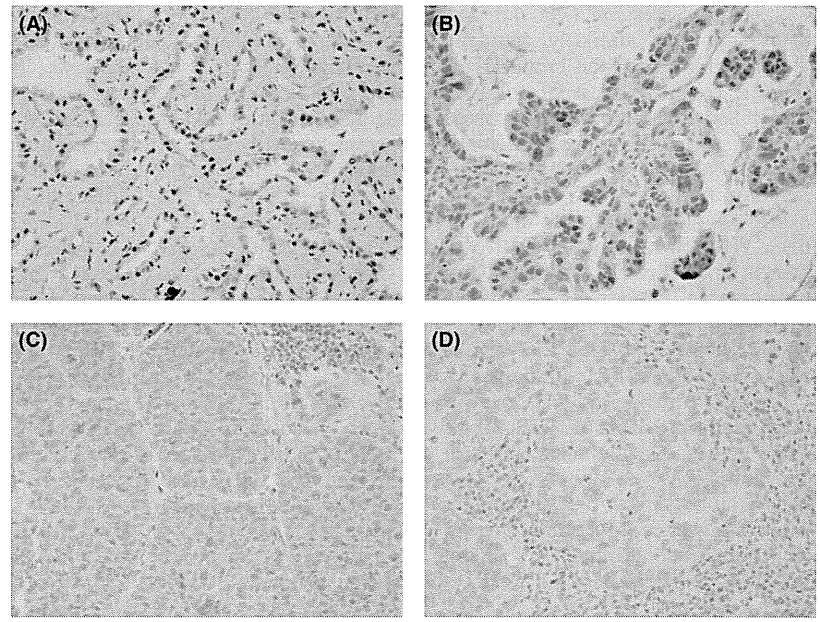

Fig. 3. BRM expressions in lung adenocarcinomas. Overall, more than 80% of cases showed positivity for BRM. (A) Lepidic growth components showed strong immunoreactivity for BRM. (B) Moderately differentiated adenocarcinomas, such as papillary adenocarcinoma, also often show positivity for BRM. (C) Solid adenocarcinoma with mucin frequently showed negative or weak staining for BRM. (D) Some cases with papillary or acinar morphology show negative staining for BRM. Note BRM positivity in stromal cells.

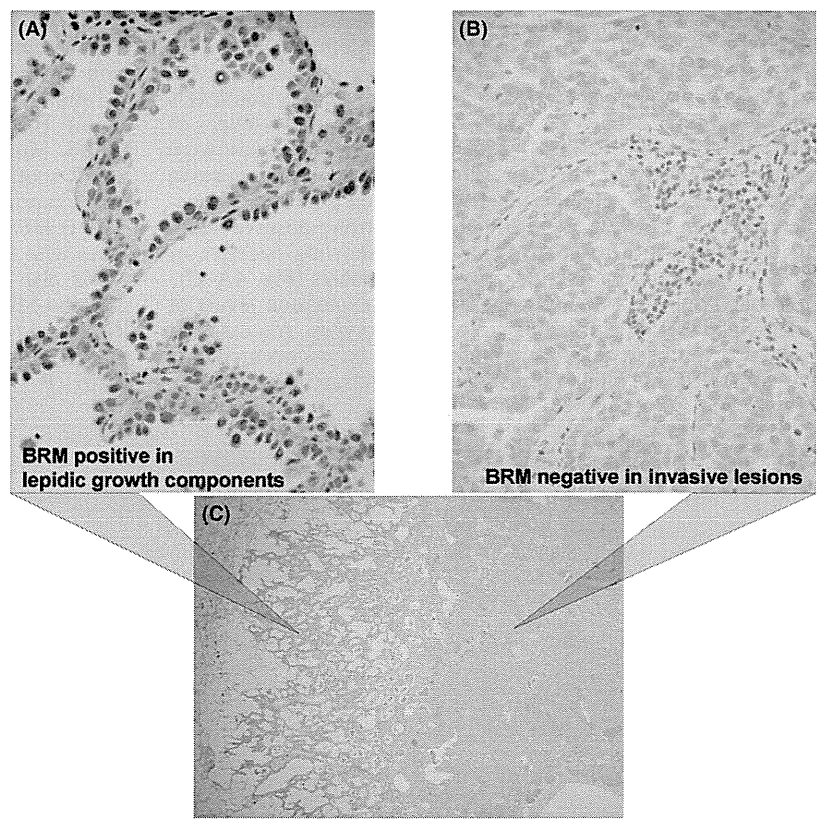

Fig. 4. Heterogeneous BRM expression in lung adenocarcinoma. (A) High-power field of lepidic growth components, which show strong positivity for BRM. (B) High-power field of invasive acinar components, which show negative positivity for BRM. (C) Low-power field of invasive adenocarcinoma with lepidic growth components; left side shows lepidic growth components, and right side shows invasive acinar components.

of MET tended to be low in cases with loss of BRG1 and BRM, but the difference was not significant.

BRM loss was significantly more frequent in heavy smokers and in cases with vessel invasion ($P = 0.0093$ and $P = 0.0002$, respectively; Table 3). BRG1 loss was significantly correlated with pleural invasion and pleural dissemination ($P = 0.0471$ and $P = 0.0449$, respectively; Table 3).

Prognostic significance of the expressions of BRG1 and BRM. Lastly, we performed hierarchical cluster analysis using the publicly available data of 442 primary lung adenocarcinoma cases,[15] based on the gene expressions of BRG1, BRM, TTF-1, MUC1, CK7, E-cadherin, and vimentin. Results are shown in Figure 5(A). Principally, primary lung adenocarcinoma cases could be classified into two groups: (i) tumors

Table 2. Correlations between expression levels of BRG1 and BRM and histopathological subtypes of primary lung adenocarcinomas

	BRG1 high BRM high	BRG1 low BRM high	BRG1 high BRM low	BRG1 low BRM low	Total
Non-mucinous adenocarcinoma *in situ*	8	0	0	0	8
Minimally invasive adenocarcinoma	12	0	0	0	12
Invasive adenocarcinoma, lepidic predominant	9	0	0	0	9
Invasive adenocarcinoma, acinar predominant	8	0	2	1	11
Invasive adenocarcinoma, papillary predominant	29	3	3	0	35
Invasive mucinous adenocarcinoma	2	1	0	0	3
Colloid adenocarcinoma	1	0	0	0	1
Invasive adenocarcinoma, micropapillary predominant	1	0	0	0	1
Invasive adenocarcinoma, solid predominant	1	2	6	4	13
Total	71	6	11	5	93

Table 3. Correlations between expression levels of BRG1 and BRM and clinico-pathological factors

	BRG1 expression			BRM expression		
	High	Low	*P*-value	High	Low	*P*-value
Pathological stage						
I	60	7	0.5082	57	10	0.3499
II + III + IV	22	4		20	6	
T-stage						
T1	52	5	0.2508	48	9	0.6492
T2, T3, T4	30	6		29	7	
Nodal involvement†						
Positive	20	1	0.3608	17	4	0.7381
Negative	61	8		58	11	
Lymphatic invasion						
Positive	22	1	0.2004	18	5	0.5066
Negative	60	10		59	11	
Vessel invasion						
Positive	23	5	0.2373	17	11	0.0002
Negative	59	6		60	5	
Pleural invasion						
Positive	21	6	0.0471	21	6	0.4122
Negative	61	5		56	10	
Dissemination						
Positive	3	2	0.0449	4	1	0.8648
Negative	79	9		73	15	
Pulmonary metastasis						
Positive	4	0	0.4540	4	0	0.3514
Negative	78	11		73	16	
Lepidic growth						
Present	65	0	<0.0019	59	6	0.0019
Absent	17	11		18	10	
Smoking Index						
≤600	26	6	0. 1344	22	10	0.0093
>600	56	5		55	6	

†Pathological N-factors were not determined for three cases of stage IV patients with pleural dissemination. Underlined values are $P < 0.05$.

Table 4. Correlations between expression levels of BRG1 and BRM and genetic status of EGFR and KRAS and expression levels of E-cadherin, TTF-1, CK7, MUC1, phopsho-MET, and phospho-EGFR

	BRG1 expression			BRM expression		
	High	Low	*P*-value	High	Low	*P*-value
EGFR mutations						
Positive	45	0	0.0006	39	6	0.3382
Negative	37	11		38	10	
KRAS mutations						
Posivite	5	2	0.1537	4	3	0.0615
Negative	77	9		73	13	
E-cadherin						
High	81	3	<0.0001	72	12	0.0227
Low	1	8		5	4	
TTF-1						
High	62	0	<0.0001	57	5	0.0010
Low	20	11		20	11	
CK7						
High	74	4	<0.0001	67	11	0.0707
Low	8	7		10	5	
MUC1(membranous)						
High	63	3	0.0007	62	4	<0.0001
Low	19	8		15	12	
MUC1(depolarized)						
High	7	3	0.0596	4	6	0.0001
Low	79	8		73	10	
Phospho-EGFR						
High	69	4	0.0003	67	6	<0.0001
Low	13	7		10	10	
Phospho-MET						
High	19	2	0.7102	19	2	0.2892
Low	63	9		28	14	

Underlined values are $P < 0.05$.

showing high expression levels of TTF-1, MUC1 and E-cadherin, and low expression levels of vimentin, and (ii) tumors showing low expression levels of TTF-1, MUC1 and E-cadherin, and high expression levels of vimentin (Fig. 5A). High expression levels of both BRG1 and BRM were frequently seen in the former, while low expression levels of either of or both BRG1 and BRM were frequently seen in the latter (Fig. 5A). These results confirm and reinforce data from cancer cell lines and primary lung adenocarcinoma cases in our institution.

To ascertain the prognostic significance of the expressions of BRG1 and BRM in lung adenocarcinoma, we undertook a survival analysis using the Kaplan–Meier method. We separated 442 lung adenocarcinoma cases into three groups based on the gene expression levels of BRG1 and BRM; (i) cases with high expression (more than or equal to the average); (ii) cases with moderate expression (under the average, and more than or equal to half the average); and (iii) cases with low expression (under half the average). Results are shown in Figure 5(B). High expression of BRG1 and BRM both correlated significantly with better prognosis. Figure 5(C) also shows patient survival curves for the four groups: (i) BRG1-high and BRM-high; (ii) BRG1-high and BRM-low; (iii) BRG1-low and BRM-high; and (iv) BRG1-low and BRM-low. The BRG1-low and BRM-low group showed significantly poorer prognosis than the other groups.

doi: 10.1111/cas.12065

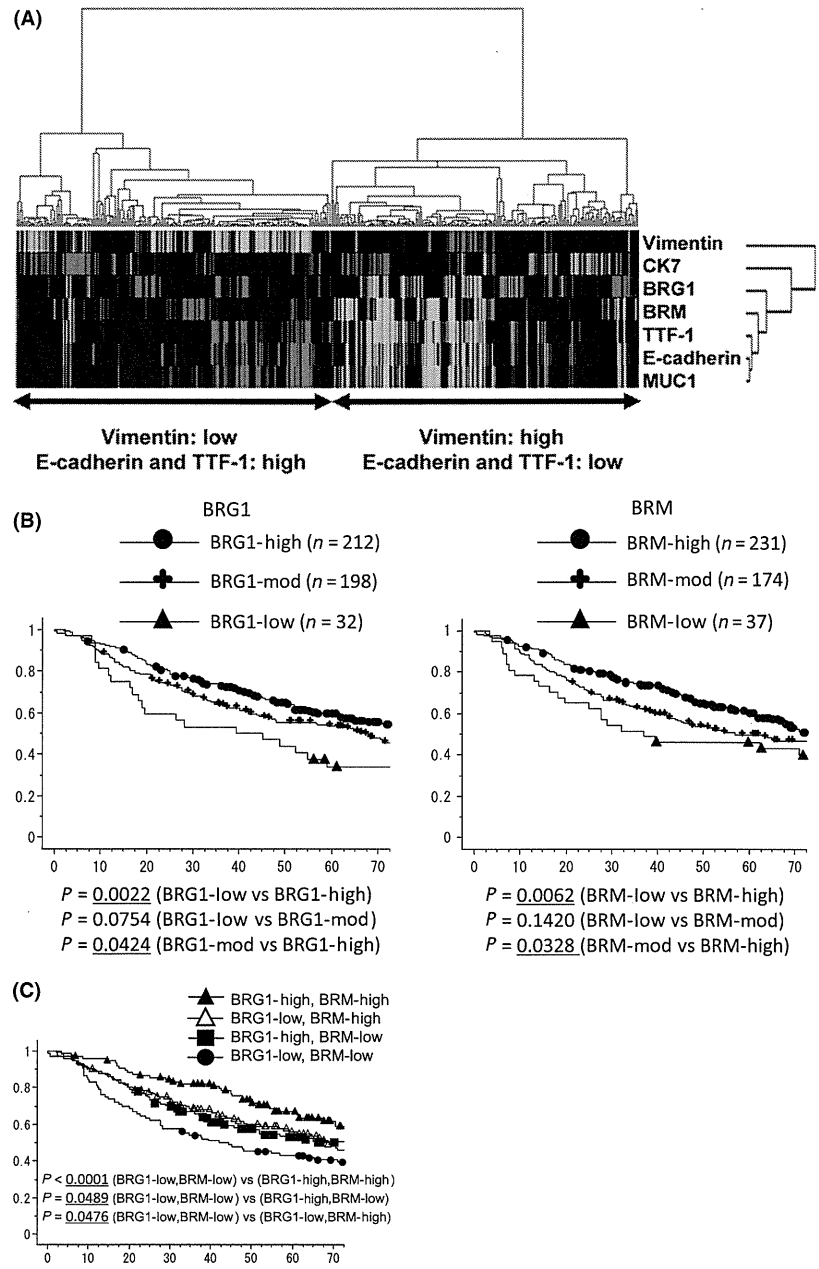

Fig. 5. Analysis of the publicly available data of 442 primary lung adenocarcinoma cases. (A) Hierarchical cluster analysis using the gene expressions of vimentin, CK7, BRG1, BRM, TTF-1, E-cadherin, and MUC1. (B) Patient survival according to the expression levels of BRG1 and BRM. Lung adenocarcinoma cases were separated into three groups based on gene expression levels of BRG1 and BRM: (i) cases with high expression (more than or equal to the average); (ii) cases with moderate expression (under the average, and more than or equal to half the average); and (iii) cases with low expression (under half the average). Left panel shows patient survival curves with high expression levels of BRG1 (BRG1-High), moderate expression levels of BRG1 (BRG1-Mod), and low expression levels of BRG1 (BRG1-Low). Right panel shows patient survival curves with high expression levels of BRM (BRM-High), moderate expression levels of BRM (BRM-Mod), and low expression levels of BRM (BRM-Low). (C) Patient survival according to the expression pattern of BRG1 and BRM. Patients were separated into four groups according to the expression pattern of BRG1 and BRM as follows: cases with high expression levels of both BRG1 and BRM (BRG1-High, BRM-High), cases with high expression levels of BRG1 and moderate or low expression levels of BRM (BRG1-High, BRM-Low), cases with moderate or low expression levels of BRG1 and high expression levels of BRM (BRG1-Low, BRM-High), the cases with moderate or low expression levels of both BRG1 and BRM (BRG1-Low, BRM-Low).

Discussion

This is, to our knowledge, the first report demonstrating the tight correlation between loss of BRG1 and BRM and EMT in cancer. Results of this study also confirm and reinforce our previous data that loss of the bronchial epithelial phenotype occurs in lung adenocarcinomas with EMT features.[13]

Recent studies show that loss of another component of the SWI/SNF chromatin remodeling complex, BAF250A (ARID1A), was frequent in high-grade endometrial carcinomas and clear cell carcinomas of the ovary[16] and that loss of the BAF250A protein correlates with the ARID1A mutation status.[17,18] Interestingly, there appears to be a similarity between loss of BRG1 and that of ARID1A; both tend to occur in high-grade tumors or in tumors with an altered epithelial phenotype.

Another interesting finding of this study was that features of TRU type lung adenocarcinomas,[14] that is, lepidic growth features, high expression levels of the TTF-1 protein, and EGFR mutations were absent in all cases with loss of the BRG1 protein. In tumors with BRG1 loss, BRG1 protein expression was typically absent in almost all cancer cells. These results suggest that loss of BRG1 occurs at an early step of carcinogenesis of lung adenocarcinoma with the mesenchymal-like phenotype, that is, a subset of non-TRU type lung adenocarcinomas with EMT features.

All cases with concomitant loss of BRG1 and BRM were devoid of lepidic growth components, harbored no EGFR mutations, and correlated more with solid adenocarcinoma morphology than a single loss of BRG1 or BRM, which suggested that loss of BRM may also occur in a subset of the mesenchymal-like phenotype, simultaneously with, or subsequently to, loss of BRG1, and may accelerate poorer

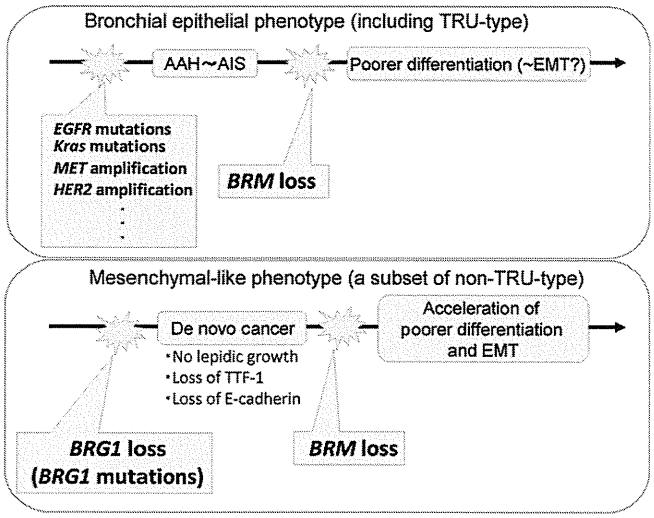

Fig. 6. Hypothetical schemes of BRG1 and BRM loss in the development of two types of lung adenocarcinomas: lung adenocarcinoma with the bronchial epithelial phenotype (upper panel) and lung adenocarcinoma with mesenchymal-like phenotype (lower panel).

differentiation and EMT and lead to the more malignant phenotype. The survival analysis of Shedden's data, which showed that cases with concomitant loss of BRG1 and BRM had poorer prognosis than cases with a single loss of BRG1, supports this hypothesis.

BRM expression was positive in lepidic growth components, but was weak or absent in invasive poorer differentiated lesions, such as solid components. In contrast to BRG1 loss, BRM loss may occur during the progressions of lung adenocarcinomas with the bronchial epithelial phenotype. Figure 6 shows our hypothetical schemes for BRG1 and BRM loss in the development of two types of lung adenocarcinomas: lung adenocarcinomas showing the bronchial epithelial phenotype and those showing the mesenchymal-like phenotype.

BRG1 and BRM regulate a broad range of genetic programs, including cell differentiation and proliferation, and it has been suggested that SWI/SNF complexes may dictate lineage-specific chromatin remodelling functions and act as master regulators of the master regulators.[4] Thus, although the exact mechanism by which loss of BRG1 and BRM leads to tumor development and EMT is unknown, loss of BRG1 and BRM may cause uncontrolled cellular proliferation and disrupt the differentiation program of bronchial epithelial cells,[19] resulting in formation of tumors with loss of expression of CK7, MUC1, and TTF-1. Why BRG1 loss occurs exclusively in the progression of EGFR wild-type tumor is currently unknown. One speculation could be that the simultaneous presence of EGFR mutation and BRG1 loss is for some reason incompatible with survival of cancer cells. Finally, we speculate that epigenetic therapy aiming to restore the functions of BRG1 and BRM would be a possible new therapy for treating tumors with EMT features.

Acknowledgments

This study was supported in part by the Smoking Research Foundation, the Foundation for Development of Community, the Vehicle Racing Commemorative Foundation, and the Ministry of Health, Labor and Welfare, and the Ministry of Education, Culture, Sports, Science and Technology of Japan. This publication was subsidized by JKA through its promotion funds from KEIRIN RACE. We thank Dr S. Matsukuma and Dr E. Tsuchiya, Molecular Pathology and Genetics Division, Kanagawa Cancer Center Research Institute, for technical advice on the loop-hybrid method.

Disclosure Statement

The authors have no conflict of interest.

References

1 Statistics and Information Department. *Vital Statistics, 2000*. Tokyo: Ministry of Health, Labor and Welfare, 2001.
2 Jemal A, Siegel R, Ward E *et al.* Cancer statistics, 2006. *CA Cancer J Clin* 2006; **56**: 106–30.
3 Janku F, Garrido-Laguna I, Petruzelka LB, Stewart DJ, Kurzrock R. Novel therapeutic targets in non-small cell lung cancer. *J Thorac Oncol* 2011; **6**: 1601–12.
4 Wilson BG, Roberts CW. SWI/SNF nucleosome remodellers and cancer. *Nat Rev Cancer* 2011; **11**: 481–92.
5 Jones S, Wang TL, Shih IM *et al.* Frequent mutations of chromatin remodeling gene ARID1A in ovarian clear cell carcinoma. *Science* 2010; **330**: 228–31.
6 Varela I, Tarpey P, Raine K *et al.* Exome sequencing identifies frequent mutation of the SWI/SNF complex gene PBRM1 in renal carcinoma. *Nature* 2011; **469**: 539–42.
7 Gui Y, Guo G, Huang Y *et al.* Frequent mutations of chromatin remodeling genes in transitional cell carcinoma of the bladder. *Nat Genet* 2011; **43**: 875–8.
8 Zang ZJ, Cutcutache I, Poon SL *et al.* Exome sequencing of gastric adenocarcinoma identifies recurrent somatic mutations in cell adhesion and chromatin remodeling genes. *Nat Genet* 2012; **44**: 570–4.
9 Medina PP, Romero OA, Kohno T *et al.* Frequent BRG1/SMARCA4-inactivating mutations in human lung cancer cell lines. *Hum Mutat* 2008; **29**: 617–22.
10 Glaros S, Cirrincione GM, Palanca A, Metzger D, Reisman D. Targeted knockout of BRG1 potentiates lung cancer development. *Cancer Res* 2008; **68**: 3689–96.
11 Reisman DN, Sciarrotta J, Wang W, Funkhouser WK, Weissman BE. Loss of BRG1/BRM in human lung cancer cell lines and primary lung cancers: correlation with poor prognosis. *Cancer Res* 2003; **63**: 560–6.
12 Fukuoka J, Fujii T, Shih JH *et al.* Chromatin remodeling factors and BRM/BRG1 expression as prognostic indicators in non-small cell lung cancer. *Clin Cancer Res* 2004; **10**: 4314–24.
13 Matsubara D, Ishikawa S, Sachiko O *et al.* Co-activation of epidermal growth factor receptor and c-MET defines a distinct subset of lung adenocarcinomas. *Am J Pathol* 2010; **177**: 2191–204.
14 Takeuchi T, Tomida S, Yatabe Y *et al.* Expression profile-defined classification of lung adenocarcinoma shows close relationship with underlying major genetic changes and clinicopathologic behaviors. *J Clin Oncol* 2006; **24**: 1679–88.
15 Shedden K, Taylor JM, Enkemann SA *et al.* Gene expression-based survival prediction in lung adenocarcinoma: a multi-site, blinded validation study. *Nat Med* 2008; **14**: 822–7.
16 Wiegand KC, Lee AF, Al-Agha OM *et al.* Loss of BAF250a (ARID1A) is frequent in high-grade endometrial carcinomas. *J Pathol* 2011; **224**: 328–33.
17 Wiegand KC, Shah SP, Al-Agha OM *et al.* ARID1A mutations in endometriosis-associated ovarian carcinomas. *N Engl J Med* 2010; **363**: 1532–43.
18 Maeda D, Mao TL, Fukayama M *et al.* Clinicopathological significance of loss of ARID1A immunoreactivity in ovarian clear cell carcinoma. *Int J Mol Sci* 2010; **11**: 5120–8.
19 Richly H, Lange M, Simboeck E, Di Croce L. Setting and resetting of epigenetic marks in malignant transformation and development. *BioEssays* 2010; **32**: 669–79.

doi: 10.1111/cas.12065

Supporting Information

Additional Supporting Information may be found in the online version of this article:

Data S1. Gene expression data of 19 cell lines.

Doc. S1. Supporting information about materials and methods.

Fig. S1. Gene and protein level expressions of BRG1, BRM, etc. of EGFR-mutated cell lines.

Fig. S2. Immunostaining for BRG1, BRM and E-cadherin in serial sections.

Identification of CCDC6-RET Fusion in the Human Lung Adenocarcinoma Cell Line, LC-2/ad

Daisuke Matsubara MD, PhD,† Yoshihiko Kanai,‡ Shumpei Ishikawa, MD, PhD,§ Shiori Ohara, BSc,* Taichiro Yoshimoto, MD, PhD,* Takashi Sakatani, MD, PhD,* Sachiko Oguni,* Tomoko Tamura,* Hiroaki Kataoka, MD, PhD,‖ Shunsuke Endo, MD, PhD,‡ Yoshinori Murakami, MD, PhD,† Hiroyuki Aburatani, MD, PhD,¶ Masashi Fukayama, MD, PhD,§ and Toshiro Niki, MD, PhD**

Rearranged during transfection (*RET*) fusions have been newly identified in approximately 1% of patients with primary lung tumors. However, patient-derived lung cancer cell lines harboring *RET* fusions have not yet been established or identified, and therefore, the effectiveness of an RET inhibitor on lung tumors with endogenous *RET* fusion has not yet been studied. In this study, we report identification of *CCDC6-RET* fusion in the human lung adenocarcinoma cell line LC-2/ad. LC-2/ad showed distinctive sensitivity to the RET inhibitor, vandetanib, among 39 non–small lung cancer cell lines. The xenograft tumor of LC-2/ad showed cribriform acinar structures, a morphologic feature of primary *RET* fusion–positive lung adenocarcinomas. LC-2/ad cells could provide useful resources to analyze molecular functions of RET-fusion protein and its response to *RET* inhibitors.

Key Words: RET fusion, Lung adenocarcinoma, Cell line, Vandetanib.

(*J Thorac Oncol.* 2012;7: 1872–1876)

Lung cancer is the leading cause of cancer mortality in developed countries. Molecularly targeted therapy is a new therapeutic modality now under intense investigation.[1] *KRAS* mutations, epidermal growth factor receptor (*EGFR*) mutations, and anaplastic lymphoma receptor tyrosine kinase (*ALK*) fusions are well-known driver mutations identified in individuals with lung adenocarcinoma. Molecular analyses have demonstrated that *EGFR*-mutated non–small-cell lung tumors are usually sensitive to the EGFR inhibitors gefitinib and erlotinib, and *ALK* fusion non–small-cell lung tumors are sensitive to the ALK inhibitor crizotinib. Lung tumors with *ROS1* fusions also respond to crizotinib.[2]

Recently, several independent studies newly identified *RET* fusions (*KIF5B-RET* or *CCDC6-RET*) in approximately 1% of patients with primary lung tumors.[3–9] *RET* fusions were mutually exclusive of *EGFR*, *KRAS*, and *ALK* mutations. Although these studies suggested that RET kinase inhibitors would be effective for a subgroup of lung tumors harboring *RET* fusions, the clinical benefits of RET kinase inhibitors in these patients have not been clarified yet. Studies using patient-derived lung cancer cell lines harboring *RET* fusions are now needed to decide the best optimal drug treatments; however, lung cancer cell lines with endogenous *RET* fusions have not been established nor identified to date.[10]

In this study, we found that a lung adenocarcinoma cell line, LC-2/ad, harbored *CCDC6-RET* fusion, and examined its sensitivity to vandetanib, a multikinase inhibitor of RET, vascular endothelial growth factor receptor-2, and EGFR. To the best of our knowledge, this is the first report to identify a patient-derived lung cancer cell line harboring *RET* fusion and demonstrate its sensitivity to a RET kinase inhibitor. The availability of this cell line would facilitate studies on optimal drug treatments and the biological properties of *RET* fusion–positive lung adenocarcinomas.

MATERIALS AND METHODS

Cell Lines and Medium

We used 39 non–small-cell lung cancer cell lines, 34 adenocarcinoma cell lines (H23, H292, H358, H441, H522, H596, H650, H1395, H1648, H1650, H1651, H1703, H1781, H1793, H1838, H1975, H1993, H2009, H2087, H2228, H2405, HCC827, HCC4006, Calu-3, A549, ABC1, PC3, VMRC-LCD, RELF-LC-Ad1, RELF-LC-Ad2, HLC-1, LC-2/ad, RERF-LC-KJ, and L27), four large-cell carcinoma cell lines (Lu65, H460, H661, and H1299), and one adenosquamous cell line (H596). Detailed information on

*Department of Pathology, Division of Integrative Pathology, Jichi Medical University, Shimotsuke, Tochigi, Japan; †Department of Cancer Biology, Division of Molecular Pathology, The Institute of Medical Science, The University of Tokyo, Minato-ku, Tokyo; ‡Department of Surgery, Division of General Thoracic Surgery, Jichi Medical University, Tochigi, Japan; §Department of Human Pathology, Graduate School of Medicine, The University of Tokyo, Bunkyo-ku Tokyo; ‖Department of Pathology, Faculty of Medicine, University of Miyazaki, Miyazaki, Japan; and ¶Laboratory for Systems Biology and Medicine, Division of Genome Science, Research Center for Advanced Science and Technology, The University of Tokyo, Meguro-ku, Tokyo, Japan.

Disclosure: T.N. and D.M. are recipients of the AstraZeneca research award 2007. The authors declare no conflict of interest.

Address for correspondence: Toshiro Niki, MD, Department of Integrative Pathology, Jichi Medical University, 3311-1 Yakushiji, Shimotsuke-shi, Tochigi, 329–0498, Japan. E-mail: tniki@jichi.ac.jp00002012

ISSN: 1556-0864/12/0712-1872

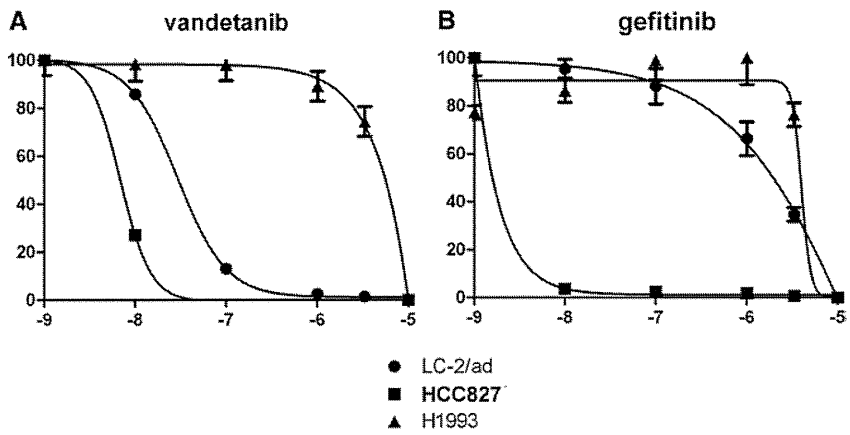

FIGURE 1. Dose-response curves of three cell lines, LC-2/ad, HCC827, and H1993. HCC827 harbors *EGFR* Exon 19 deletion (746–750) and H1993 expresses wild-type *EGFR*. The *x* axis indicates the log10 (concentration of vandetanib [*A*] and gefitinib [*B*]), and the *y* axis indicates the % of cell viability = (mean absorbance in test wells)/(mean absorbance in control well) × 100. *A*, LC-2/ad and HCC827 were sensitive to vandetanib (IC50 values were 2.9E-08 and 6.9E-09, respectively), but H1993 was resistant to vandetanib (IC50 value was 5.1E-04). *B*, HCC827 was sensitive to gefitinib (inhibitory concentration 50 value was 1.8E-10), but LC-2/ad and H1993 were resistant to gefitinib (inhibitory concentration 50 values were 1.8E-05 and 4.0E-06, respectively). EGFR, epidermal growth factor receptor.

the 39 cell lines is available in our previous reports.[11,12] Among the 39 cell lines, *EGFR* mutations were detected in five cell lines: HCC827, HCC4006, PC3, H1650, and H1975. *EGFR* mutation status of the five cell lines (Supplementary Table 1, Supplemental Digital Content 1, http://links.lww.com/JTO/A337). We have not checked the 39 cell lines for *ALK* fusion in our hands, but H2228 has been reported to harbor *ALK* fusion[13] (Supplementary Table 1, Supplemental Digital Content 1, http://links.lww.com/JTO/A337).

RET Fusion–Specific Polymerase Chain Reaction

We used fusion-specific reverse-transcriptase polymerase chain reaction (RT-PCR) with the forward primer, *CCDC6*-197F (5′-TGCAGCAAGAGAACAAGGTG-3′), the forward primer, *KIF5B*-867F (5′-ATCCAGTTCGTCCTGTTCAGAGC-3′), *KIF5B*-2265R (5′-AGCCACAGATCAGGAAAAGA-3′), and reverseprimer,*RET*-2381R(5′-CAGGCCCCATACAATTTGAT-3′), following the method by Takeuchi et al.[4]

Genetic and Protein Analysis of Cell Lines

The DNA, RNA, and cell lysates were prepared from cell lines by standard procedures. Experimental details of sequencing, copy number analyses, and Western blotting are given in our previous reports [11,12] (antibodies for Western blotting are listed in Supplementary Table 1, Supplemental Digital Content 1, http://links.lww.com/JTO/A337).

Cell-Proliferation Assay

Cell viability was measured by the Cell Counting Kit-8 assay (Dojindo, Kumamoto, Japan) following the manufacturer's instructions.[11]

Xenograft Tumor of LC-2/ad

We established a xenograft tumor of LC-2/ad by injecting cell suspensions (5×10^6) into the flank of a 6-week-old female severe combined immunodeficient mouse NOD C.B-17-Prkdc scid/J (NOD/SCID).

Immunohistochemistry

A formalin-fixed, paraffin-embedded xenograft tumor specimen of LC-2/ad was analyzed by immunohistochemistry using antibodies to RET, TTF-1, Napsin A, and thyroglobulin (sources of antibodies are given in Supplementary Table 2, Supplemental Digital Content 5, http://links.lww.com/JTO/A341).

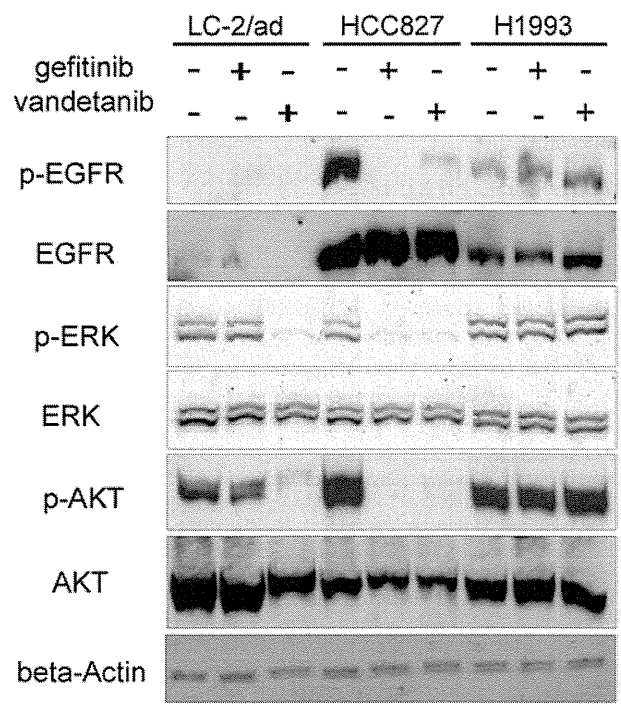

FIGURE 2. Effects of vandetanib and gefitinib on the phosphorylation levels of EGFR, ERK, and AKT in LC-2/ad, HCC827, and H1993. Gefitinib efficiently led to dephosphorylation of EGFR, ERK, and AKT in HCC827, but not in LC-2/ad and H1993. Vandetanib efficiently led to dephosphorylation of ERK and AKT in LC-2/ad and HCC827, but not in H1993.EGFR, EGFR, epidermal growth factor receptor; ERK, extracellular signal-regulated kinase; AKT, v-akt murine thymoma viral oncogene homolog 1.

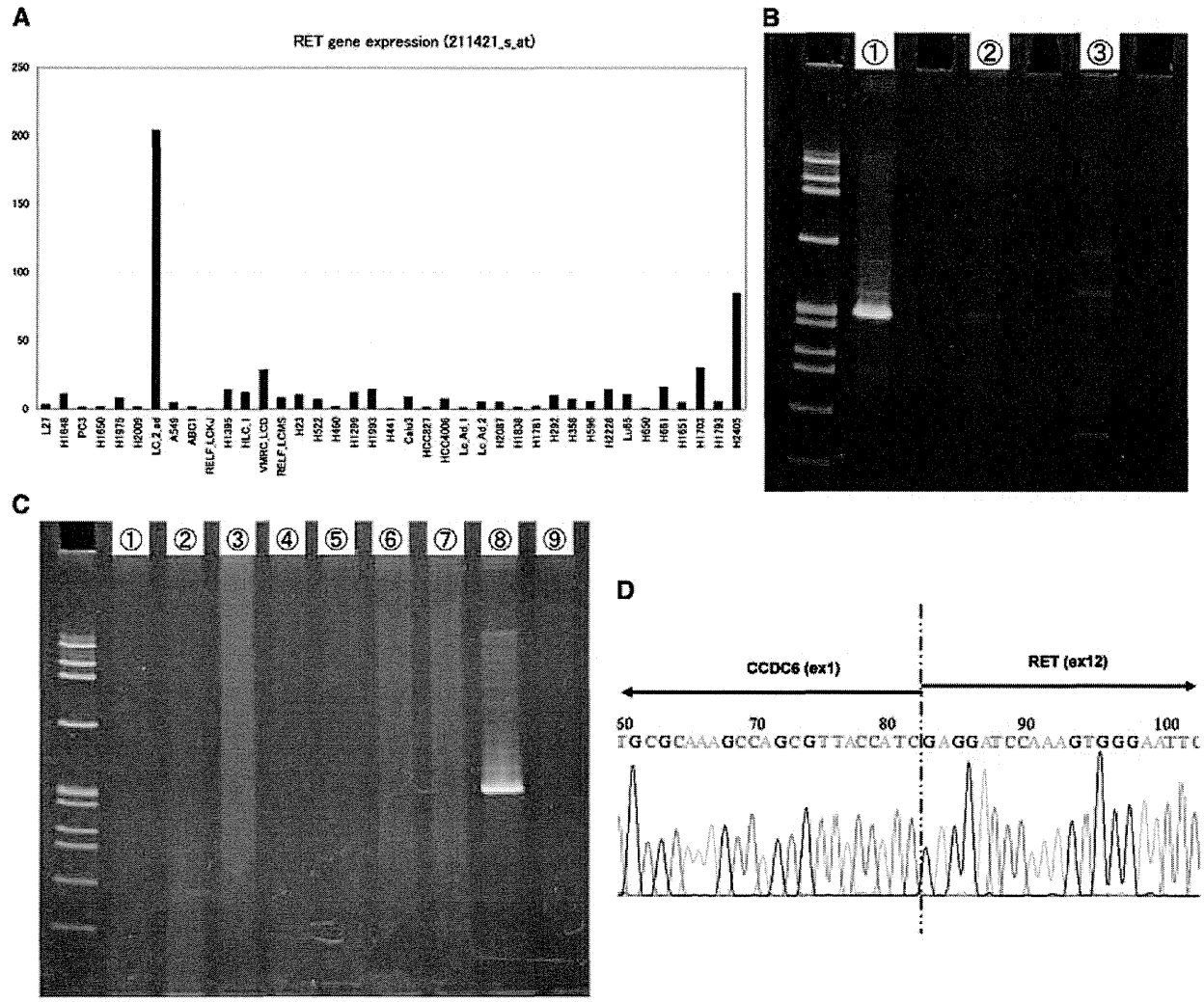

FIGURE 3. Identification of *CCDC6-RET* fusion in LC-2/ad by fusion-specific RT-PCR. *A*, Bar graphs of gene-level expressions of RET in the 39 cell lines. *B*, Results for fusion-specific RT-PCR of LC-2/ad: with the forward primer *CCDC6*-197F and reverse primer *RET*-2381R (Lane 1), with the forward primer *KIF5B*-867F and reverse primer *RET*-2381R (Lane 2), and with the forward primer KIF5B-2265F and reverse primer *RET*-2381R (Lane 3). A PCR product of an expected size (352 base pair) was amplified in Lane 1, but not in Lane 2 or Lane 3. Molecular weight marker: φX174-HAE digest. *C*, RET-CCDC6 fusion was captured only in LC-2/ad and was not captured in any of the other cell lines tested. The results for eight cell lines are shown: Lane 1, A549; Lane 2, ABC1; Lane 3, Calu-3; Lane 4, PC3; Lane 5, RERF-LC-KJ; Lane 6, HLC-1; Lane 7, L27; Lane 8, LC-2/ad; and Lane 9, VMRC-LCD). Molecular weight marker: φX174-HAE digest. *D*, Direct sequencing of the PCR product containing *RET-CCDC6* fusion. PCR, polymerase chain reaction; RT-PCR, reverse-transcriptase polymerase chain reaction.

RESULTS AND DISCUSSION

Sensitivity of Non–Small-Cell Carcinoma Cell Lines to Vandetanib and Gefitinib

We examined and compared the efficacy of vandetanib (ZD6474) and gefitinib (both provided by AstraZeneca, London, England) in 39 non–small lung carcinoma cell lines (Supplementary Figure 1, Supplemental Digital Content 2, http://links.lww.com/JTO/A338). Most cell lines showed similar sensitivities to the two kinase inhibitors; however, a notable exception was the lung adenocarcinoma, LC-2/ad, which was resistant to gefitinib, but highly sensitive to vandetanib. To illustrate this distinctive feature of LC-2/ad, the dose-response curves of LC-2/ad for gefitinib and vandetanib are shown in Figure 1, together with those of HCC827 (an *EGFR*-mutated cell line) and H1993 (an *MET*-amplified cell line).

Effects of Vandetanib on the Phosphorylation of Downstream Effectors of Growth Factor Receptors, ERK and AKT of LC-2/ad

We tested the effects of vandetanib and gefitinib treatments on ERK and AKT signaling in LC-2/ad, HCC827, and H1993. Results are shown in Figure 2. Vandetanib (1×10^{-6} M) effectively abolished baseline phosphorylation of ERK and AKT in both LC-2/ad and HCC827, but not in H1993. In

contrast, gefitinib effectively abolished baseline phosphorylation of ERK and AKT only in HCC827. This suggests that, in LC-2/ad, ERK and AKT are activated through a vandetanib-sensitive pathway other than EGFR signaling.

Identification of *RET* Fusion in LC-2/ad.

Among the tyrosine kinases targeted by vandetanib, RET was an obvious candidate molecule. First, in our oligonucleotide array analysis data of 39 cell lines, LC/2-ad showed lower expressions of vascular endothelial growth factor receptor-2 and EGFR, but distinctively higher expression of RET than that of other cell lines (Fig. 3A and Supplementary Data 1, Supplemental Digital Content 3, http://links.lww.com/JTO/A339). Second, the result of an independently performed exon array analysis of LC-2/ad suggested the existence of *RET* fusion in LC-2/ad (not shown).

To directly demonstrate *RET* fusion in LC-2/ad, we performed fusion-specific RT-PCR with primers sets that detect *RET-CCDC6* or *RET-KIF5B* (see Materials and Methods).[4] *RET-CCDC6* fusion, but not *RET-KIF5B* fusion, was detected in LC-2/ad. No PCR product was amplified in any of the other cell lines examined (Fig. 3*B* and *C*). Direct sequence analysis of RT-PCR products demonstrated a fusion between *CCDC6* exon1 and *RET* exon12 (Fig. 3*D*). An independently performed 5′ rapid amplification of complementary DNA ends (5′-RACE) using a primer complementary to *RET* demonstrated the same fusion in LC-2/ad (data not shown). Although *CCDC6-RET* fusions have now been found in many lung cancers, these cases have the same breakpoints; exon 1 of *CCDC6* is fused to exon 12 of *RET* at the cDNA level. The thyroid cancer cell line TPC-1 also harbors *CCDC6-RET* fusion at the same site.[14] However, we have not checked the breakpoints of the *RET* and *CCDC6* genes in LC-2/ad at the genomic level. Thus, it would be of interest to further determine and characterize the genomic breakpoints in *CCDC6-RET* fusion–positive tumors.

Histopathologic Characteristics of an Established Xenograft Tumor of LC-2/ad

LC-2/ad was established from the pleural effusion of a 51-year-old female pulmonary adenocarcinoma patient whose smoking status was unknown; the tumor histology was reported to be a moderately differentiated adenocarcinoma with distinct glandular structures.[15] To confirm this earlier finding and to further examine the histopathologic features of this cell line, we established a xenograft tumor of LC-2/ad

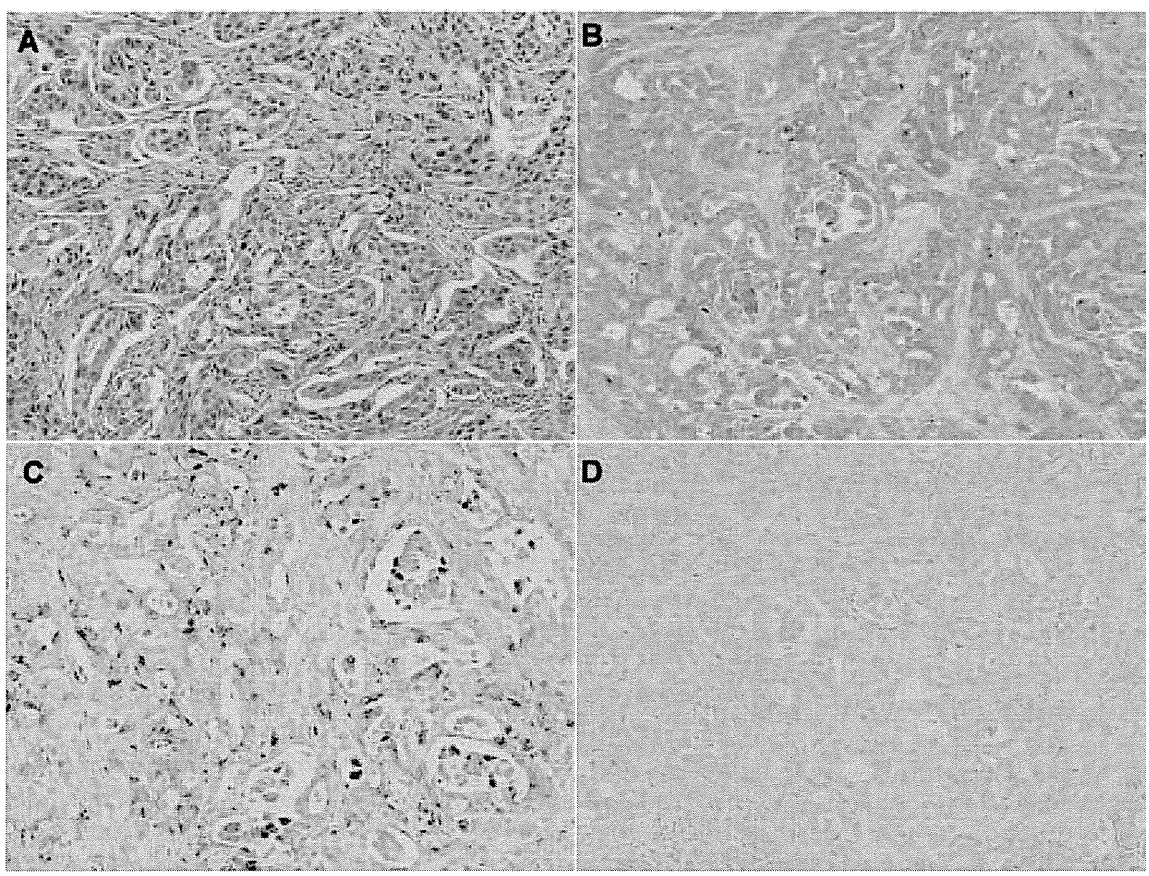

FIGURE 4. Histopathologic characteristics of an established xenograft tumor of LC-2/ad. *A*, The main histopathologic diagnosis of the tumor was acinar-predominant adenocarcinoma showing a cribriform pattern (hematoxylin and eosin staining, ×200). *B*, The tumor was positive for RET (RET immunostaining, ×200). *C*, The tumor was positive for Napsin A (Napsin A immunostaining, ×200). *D*, The tumor was negative for thyroglobulin (Thyroglobulin immunostaining, ×200).

in an NOD/SCID mouse. The results are shown in Figure 4A and Supplementary Figure 2A (Supplemental Digital Content 4, http://links.lww.com/JTO/A340). The main histopathology of the tumor was acinar-predominant adenocarcinoma showing a cribriform pattern with mucin production. This finding supports the proposal by Takeuchi et al.[4] that a cribriform acinar pattern is a distinctive histopathologic feature of kinase-fusion tumors. In the periphery of the tumor, a micropapillary component was also seen (Supplementary Figure 2B, Supplemental Digital Content 4, http://links.lww.com/JTO/A340). Immunohistochemically, the tumor was positive for RET, Napsin A, and TTF-1, but negative for thyroglobulin (Fig. 4C and 4D and Supplementary Figure 2C, Supplemental Digital Content 4, http://links.lww.com/JTO/A340), which confirmed that LC-2/ad originated from the primary lung adenocarcinoma and not from a thyroid tumor.

As far as we know, this is the first report to demonstrate that a patient-derived lung adenocarcinoma cell line harboring endogenous *RET* fusions is sensitive to vandetanib. This cell line may be a useful tool to address the following issues regarding *RET*-fusion genes. First, this cell line can be used for drug screening. We have not examined the sensitivities to the RET inhibitors other than vandetanib, but it will be interesting to test the sensitivity of LC-2/ad to sorafenib and sunitinib as well. The LC-2/ad xenografts can be also used for examination of the sensitivity in vivo. Second, this cell line may be used to study the intracellular signaling pathway of *RET* fusion in lung tumors. Third, vandetanib-resistant cell line may be generated from LC-2/ad and such a resistant subline would be invaluable in the study of the mechanisms of acquired resistance to vandetanib. Fourth, although the acinar-predominant pattern has been proposed as a morphologic feature of tumors harboring kinase fusions,[4] why kinase-fusion genes lead to such characteristic morphology is currently unclear. Thus, this cell line may provide a useful resource to study the molecular basis for the molecular–morphologic correlations in cancer.

ACKNOWLEDGMENTS

The authors thank AstraZeneca for kindly providing gefitinib and vandetanib. The authors also thank the scientists of vandetanib team of AstraZeneca for kindly reading the article.

This study was supported in part by the Ministry of Education, Culture, Sports, Science, and Technology of Japan.

REFERENCES

1. Riely GJ, Politi KA, Miller VA, Pao W. Update on epidermal growth factor receptor mutations in non-small cell lung cancer. *Clin Cancer Res* 2006;12:7232–7241.
2. Bergethon K, Shaw AT, Ou SH, et al. ROS1 rearrangements define a unique molecular class of lung cancers. *J Clin Oncol* 2012;30:863–870.
3. Kohno T, Ichikawa H, Totoki Y, et al. KIF5B-RET fusions in lung adenocarcinoma. *Nat Med* 2012;18:375–377.
4. Takeuchi K, Soda M, Togashi Y, et al. RET, ROS1 and ALK fusions in lung cancer. *Nat Med* 2012;18:378–381.
5. Lipson D, Capelletti M, Yelensky R, et al. Identification of new ALK and RET gene fusions from colorectal and lung cancer biopsies. *Nat Med* 2012;18:382–384.
6. Sasaki H, Shimizu S, Tani Y, et al. RET expression and detection of KIF5B/RET gene rearrangements in Japanese lung cancer, *Cancer Med* 2012; 22:436–445.
7. Ju YS, Lee WC, Shin JY, et al. A transforming KIF5B and RET gene fusion in lung adenocarcinoma revealed from whole-genome and transcriptome sequencing. *Genome Res* 2012;22:436–445.
8. Li F, Feng Y, Fang R, et al. Identification of RET gene fusion by exon array analyses in "pan-negative" lung cancer from never smokers. *Cell Res* 2012;22:928–931.
9. Yokota K, Sasaki H, Okuda K, et al. KIF5B/RET fusion gene in surgically-treated adenocarcinoma of the lung. *Oncol Rep* 2012;28:1187–1192.
10. Pao W, Hutchinson KE. Chipping away at the lung cancer genome. *Nat Med* 2012;18:349–351.
11. Matsubara D, Ishikawa S, Sachiko O, Aburatani H, Fukayama M, Niki T. Co-activation of epidermal growth factor receptor and c-MET defines a distinct subset of lung adenocarcinomas. *Am J Pathol* 2010;177:2191–2204.
12. Matsubara D, Ishikawa S, Oguni S, Aburatani H, Fukayama M, Niki T. Molecular predictors of sensitivity to the MET inhibitor PHA665752 in lung carcinoma cells. *J Thorac Oncol* 2010;5:1317–1324.
13. Koivunen JP, Mermel C, Zejnullahu K, et al. EML4-ALK fusion gene and efficacy of an ALK kinase inhibitor in lung cancer. *Clin Cancer Res* 2008;14:4275–4283.
14. Jossart GH, Greulich KM, Siperstein AE, Duh Q, Clark OH, Weier HU. Molecular and cytogenetic characterization of a t(1;10;21) translocation in the human papillary thyroid cancer cell line TPC-1 expressing the ret/H4 chimeric transcript. *Surgery* 1995;118:1018–1023.
15. Kataoka H, Itoh H, Seguchi K, Koono M. Establishment and characterization of a human lung adenocarcinoma cell line (LC-2/ad) producing alpha 1-antitrypsin in vitro. *Acta Pathol Jpn* 1993;43:566–573.

Laboratory Investigation (2012) 92, 1374–1385

Novel application for pseudopodia proteomics using excimer laser ablation and two-dimensional difference gel electrophoresis

Akihiko Ito[1,2,7], Takahiro Mimae[2,3,7], Ying-Shan-Zhu Yamamoto[4], Man Hagiyama[1,2], Jun Nakanishi[5], Masaoki Ito[3], Yoichiroh Hosokawa[6], Morihito Okada[3], Yoshinori Murakami[2] and Tadashi Kondo[4]

We developed a novel application to conduct pseudopodia proteomics. Pseudopodia are ventral actin-rich protrusions and play functional roles in cell migrations. Identification of pseudopodia proteins leads to a further understanding of malignant phenotypes of tumor cells and novel therapeutic strategies. In our application, tumor cells were placed on a fibronectin-coated porous membrane to form pseudopodia. According to the motile potentials of the cells, the cells formed pseudopodial microprocesses in the pores. An excimer laser, which was used for ophthalmic refractive surgeries, horizontally ablated cells at the membrane surface to remove the cell body. The microscopic observations and the protein expression studies suggested that the laser treatment caused no apparent damages to pseudopodia. Proteins in whole cells and pseudopodia fractions were individually solubilized, labeled with a highly sensitive fluorescent dye, and separated using two-dimensional difference gel electrophoresis. Among 2508 protein spots observed, 211 had different intensity between whole cells and pseudopodia fractions (more than fourfold differences and *P*-value of <0.05). The protein enrichment depended on the pore size. Mass spectrometric protein identification revealed 46 pseudopodia-localizing proteins. The localization of novel pseudopodia-localizing proteins such as RAB1A, HSP90B, TDRD7, and vimentin was confirmed using immunohistochemical examinations. The previous studies demonstrated that these four proteins may function in the cell migration process. This method will provide insights into the molecular details of pseudopodia and a further understanding of malignant phenotypes of tumor cells and novel therapeutic strategies.
Laboratory Investigation (2012) **92,** 1374–1385; doi:10.1038/labinvest.2012.98; published online 2 July 2012

KEYWORDS: excimer laser ablation; mass spectrometry; proteome; pseudopodia; two-dimensional difference gel electrophoresis

Polarized formation of pseudopodial protrusion during cell migration plays a central role in a variety of physiological and pathological processes, including embryo development, wounding healing, immunity, and cancer metastasis.[1,2] An *in vitro* model system was established to recover pseudopodia from cell bodies in order to identify signal pathways and proteins mediating cell migration.[3] In the model system, cells are plated on a porous membrane and allowed to extend pseudopodia through the pores to the ventral side of the membrane in a chemoattractant-dependent manner. To isolate the pseudopodia, the cell bodies are wiped off from the top of the membrane using a cotton-tipped swab, and proteins are extracted from the resultant membrane. Previously, mass spectrometry-based proteomics combined with this approach were used to identify numerous proteins in pseudopodia protrusions.[4–6] However, there were critical limitations to the method used in the previous report. Manual separation of pseudopodia from cell bodies created the potential for contamination of cell body components into the pseudopodial extract. Thus, a novel application to purify pseudopodia from cell bodies may provide more precise results. Additionally, the mass spectrometry-based approach described in the previous report did not allow for quantitative comparison between the cell body and pseudopodia, and

[1]Department of Pathology, Faculty of Medicine, Kinki University, Osaka, Japan; [2]Division of Molecular Pathology, Department of Cancer Biology, Institute of Medical Science, University of Tokyo, Tokyo, Japan; [3]Department of Surgical Oncology, Research Institute for Radiation Biology and Medicine, Hiroshima University, Hiroshima, Japan; [4]Division of Pharmacoproteomics, National Cancer Center Research Institute, Tokyo, Japan; [5]Nidek, Gamagori, Aichi, Japan and [6]Nara Institute of Science and Technology, Ikoma, Nara, Japan
Correspondence: Dr T Kondo, MD, PhD, Division of Pharmacoproteomics, National Cancer Center Research Institute, 5-1-1 Tsukiji, Chuo-ku, Tokyo 104-0045, Japan. E-mail: takondo@ncc.go.jp
[7]These authors contributed equally to this work.

Received 05 December 2011; revised 21 May 2012; accepted 21 May 2012

a highly sensitive and quantitative proteomics system is necessary.

We hypothesized that an excimer laser-assisted cell etching technique was a possible remedy for removing cell bodies, avoiding damages on the pseudopodia components. This technique is widely used in clinics as a tool for ophthalmic refractive surgeries such as laser-assisted *in situ* keratomileusis (LASIK). In LASIK, after the epithelium is flapped from Bowman's layer, the superficial anterior corneal tissue is reshaped by a topographically assisted excimer laser to improve myopia, hypermetropia, and astigmatism.[7] Because the excimer laser ablates living tissues in a precisely horizontal manner without causing thermal damage to the surrounding area, complications rarely occur.[8] We hypothesized that by adjusting the laser ablation front to the ventral membrane surface of the cells, the cell body could be ablated while the protrusion in the pores remain intact.

Recent advent proteomics technologies have enabled global protein expression profiling.[9] Using novel ultrahigh sensitive fluorescent dyes, gel-based protein expression studies have allowed quantitative expression profiling for a small number of cells such as those recovered by laser microdissection.[10–13] The use of multiple fluorescent dyes with different emission and excitation wavelengths for protein labeling allows inclusion of internal controls in large format gels so that highly reproducible results are expected using two-dimensional difference gel electrophoresis (2D-DIGE). We developed a proteomics system using these methods with a highly sensitive fluorescent dye and a large format gel apparatus.[10,11] We challenged biomarker development and target discovery using 2D-DIGE.[14]

In this study, we applied a combination of an excimer laser-assisted cell etching technique and 2D-DIGE to characterize proteins in pseudopodia. We identified proteins unique to pseudopodia and confirmed their localization by immunohistochemical examinations.

MATERIALS AND METHODS

Cell Culture Conditions

MDA-MB-231 human breast cancer cells, B16-F10 murine melanoma cells, murine NIH3T3 fibroblast cells, and A549 human lung adenocarcinoma cells were purchased from American Type Culture Collection (ATCC, Rockville, MD, USA). MDA-MB-231 was maintained in L-15 (Sigma-Aldrich, Gillingham, UK) supplemented with 10% FBS, 100 units/ml penicillin, 100 μg/ml streptomycin (Invitrogen, Carlsbad, CA, USA), and 0.3 g/l L-glutamine (Sigma-Aldrich). B16-F10, NIH3T3, and A549 were grown in Dulbecco's modified Eagle's medium (DMEM) (NakalaiTesque, Kyoto, Japan) supplemented with 100 units/ml penicillin, 100 μg/ml streptomycin (Invitrogen), 10 and 5% FBS, respectively. MDA-MB-231 cells were maintained at 37 °C in air and B16-F10, NIH3T3, and A549 cells were maintained in a 5% CO_2 incubator.

Preparation of Conditioned Medium

When NIH3T3 cells reached confluence, the medium was replaced with FBS-free DMEM and the cells were maintained for an additional 3 days. Next, the culture medium was filtrated and stored as conditioned medium at −80 °C.

Cell Culture on Porous Membrane

Polyethylene terephthalate (PET) membranes (BD, Franklin Lakes, NJ, USA) with pore size of 1 or 3 μm were coated with 1 μg/ml fibronectin (Sigma-Aldrich) in Dulbecco's phosphate-buffered saline (D-PBS)[15] for 30 min. After removing the fibronectin-containing D-PBS, the membrane was bottomed with a 1:1 ratio of culture medium and the above-mentioned NIH3T3-conditioned medium and the culture medium was added to the membrane.[6] Next, 1×10^5 of MDA-MB-231 cells, 1×10^4 of B16-F10 cells, and 1×10^5 of NIH3T3 cells/well were seeded in 12-well culture plate and cultured on the membrane for 2 days at 37 °C in a 5% CO_2 incubator.

Microscopic Observations

After 2 days of culture on the fibronectin-coated porous PET membrane, MDA-MB-231 and B16-F10 cells on the PET membrane were washed with PBS, fixed with 4% formalin, embedded in paraffin, and cut into sections using an SM2000R (Leica Microsystems, Wetzlar, Germany). Sections were stained using hematoxylin–eosin (HE) and observed using a light microscope (BX51, Olympus, Tokyo, Japan) equipped with a CCD camera DP72 (Olympus).

Excimer Laser Ablation and Protein Extraction

An MDA-MB-231 cell culture membrane was placed on an irradiation stage of a keratectomy system assisted by an argon fluoride excimer laser (193 nm, 10 Hz; EC-5000 CXIII, Nidek, Gamagori, Japan) adjusted for phototherapeutic keratectomy.[16,17] Laser scanning was achieved on the membrane substrate by using an image rotator mirror and exposed homogeneously on the area with a diameter of 8 mm. Laser pulse energy was adjusted to be 14 mJ, and 12 pulses were shot per scan. The laser scanning process was monitored using a CCD camera with oblique illumination. Laser scanning was manually continued until disappearing of the light scattering due to the cell bodies. To determine the scanning number, the irradiated cells and membrane were stained using HE after formalin fixation and were observed using a light microscope after mounting to examine whether the cell bodies were completely removed. The cell bodies were perfectly extracted with a scanning number of approximately 20 (range between 18 and 24). We serially processed 100 culture membrane samples. Immediately after each irradiation, the processed area of the membrane was cut using a hollow leather punch with a diameter of 5 mm and frozen in liquid nitrogen.

Protein extraction was performed from the pool of 100 frozen membranes. Briefly, the membranes were macerated,

and each protrusion lysate was prepared using lysis buffer containing 50 mM Tris-HCl (pH 7.4), 150 mM NaCl, 1% Triton X-100, 20 mM EDTA, and a protease inhibitor mixture by rotating at 4 °C. For the whole-cell lysate, 2-day cultures of MDA-MB-231 on the porous membrane were scraped, and the scraped fractions were extracted using lysis buffer. After centrifugation at 13 000 r.p.m. for 5 min at 4 °C to remove insoluble material, the supernatant was recovered and used in subsequent protein expression studies.

A schematic diagram of laser ablation and protein extraction is provided in Figure 1. The video image of laser ablation is available in Supplementary Video Data.

Immunoblotting and Silver Staining

Protein lysates from human lung tissues (P1234156 and P1234159) were purchased from BioChain Institute (Hayward, CA, USA). Protein lysates from MDA-MB-231 cells and A549 cells and human lung tissue were suspended in SDS-PAGE sample buffer containing 2% SDS, 50 mM dithiothreitol, 50 mM Tris, and 10% glycerol, and incubated at 95 °C for 5 min. The proteins were fractionated using SDS-PAGE and a 10% polyacrylamide gel. Fractionated proteins were transferred onto a polyvinyllidene difluoride membrane (Millipore, Bedford, MA, USA), blocked with 5% skim milk for 30 min, and reacted with an antibody against integrin α2 (2/CD49b,

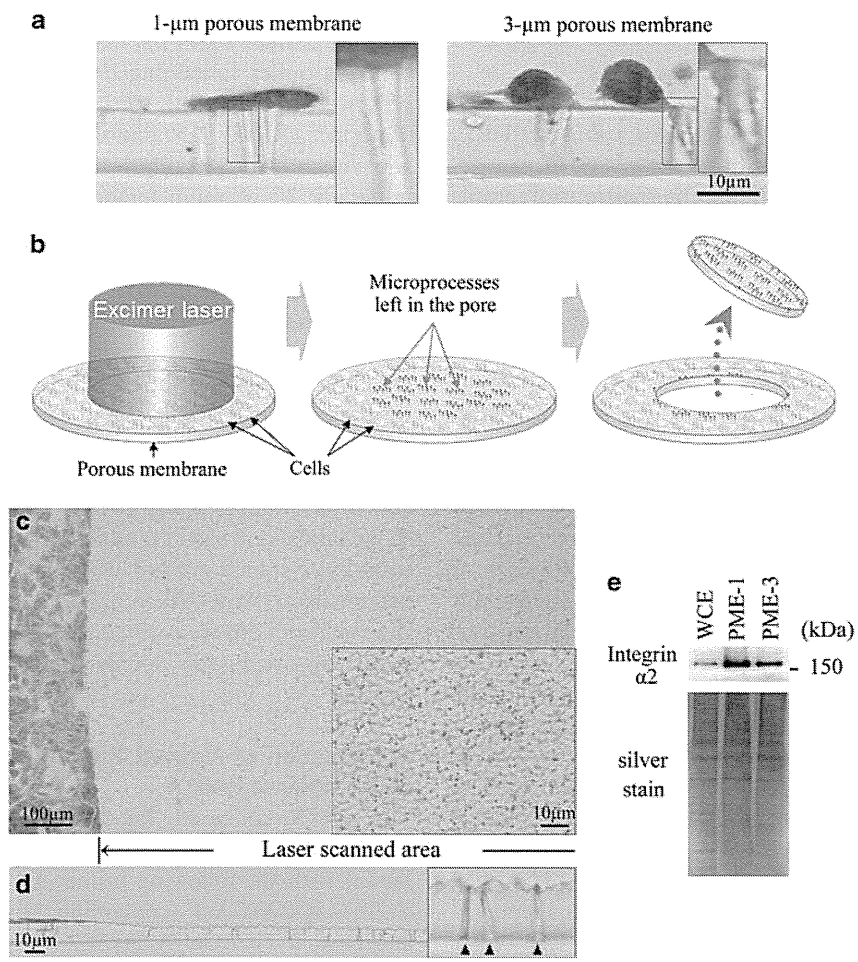

Figure 1 Microscopic observation of pseudopodia in the porous membrane. Pseudopodia in pores with diameters of 1 μm (**a**, left) or 3 μm (**a**, right). Enlarged image in the box shows pseudopodial microprocesses. A schematic diagram of excimer laser ablation is shown. The laser scanning plane was adjusted to the surface of the porous membrane (**b**, left). The pulse energy and scanning cycles were optimized to completely remove cell bodies and leave the remaining microprocesses intact in the membrane pores (**b**, middle). Membranes were punched out after ablation and frozen in liquid nitrogen (**b**, right). The membrane stained with hematoxylin–eosin (HE) was ablated, and no cell bodies remained in the ablated area. The boxed area shows the dot-like appearance of the remaining pseudopodial microprocesses (**c**). Vertical images of the whole cell and pseudopodia after laser ablation. Arrows in the box indicate pseudopodia of higher magnitude. Enlarged image in the box shows that pseudopodial microprocesses stained with HE remained intact after laser ablation (**d**). Protein extracts from 1 and 3 μm porous membranes were defined as pseudopodial microprocess extracts PME-1 and PME-3, respectively, and the whole-cell extract as WCE. Western blotting revealed highly enriched integrin α2 in PME-1 and PME-3 compared with WCE. A gel prepared in parallel was silver-stained to control for protein loading (**e**).

BD, 1:1000 dilution), RAB1A (C-19, Santa Cruz Biotechnology, Santa Cruz, CA, USA, 1:100 dilution), TDRD7 (HPA024529, Sigma-Aldrich, 1:100 dilution), HSP90B (HPA003901, Sigma-Aldrich, 1:100 dilution), and β-actin (AC-15, Sigma-Aldrich, 1:100 dilution) at 4 °C overnight. Then, the membranes were incubated with horseradish peroxidase-conjugated secondary anti-mouse antibody (Santa Cruz Biotechnology, 1:1000 dilution) for integrin $\alpha 2$ and β-actin and anti-rabbit antibody (Santa Cruz Biotechnology) for RAB1A, TDRD7, and HSP90B at 4 °C for 2 h. Protein complexes were detected using ECL Western Blotting Detection Reagents (GE Healthcare, Uppsala, Sweden). The proteins fractionated by SDS-PAGE in parallel experiments were silver-stained using the Proteo Silver™ Plus Silver Stain Kit according to the manufacture's instruction (Sigma-Aldrich).

2D-DIGE and Protein Identification by Mass Spectrometry

Protein expression profiling was achieved using 2D-DIGE with a highly sensitive fluorescent dye and a large format gel, as previously described.[10] Briefly, the internal control sample was prepared by mixing a portion of all individual samples. Next, 5 μg of the internal control sample and individual sample were labeled with Cy3 and Cy5 (CyDye DIGE Fluor saturation dye; GE Healthcare), respectively, according to our previous report.[10] These differentially labeled protein samples were mixed and separated using 2D-DIGE. The first-dimension separation was achieved using IPG DryStrip gels (24 cm in length; pI, 4–7, GE). The second-dimension separation was achieved using SDS-PAGE with a large format gel apparatus (33 cm separation distance; Biocraft, Itabashi, Tokyo, Japan). After electrophoresis, the gels were scanned using laser scanners (Typhoon Trio, GE Healthcare) at appropriate wavelengths. The intensity of the Cy5 image was normalized to that of the Cy3 image for all protein spots in the identical gel using the Progenesis SameSpot software (Nonlinear Dynamics, Newcastle upon Tyne, UK). All samples were analyzed in triplicate, and the intensity between the three gels was normalized for statistical analysis. System reproducibility was verified by comparing protein profiles obtained from three independent separations of identical samples.

Proteins corresponding to the protein spots were identified using mass spectrometry according to our previous report.[10] Briefly, MDA-MB-231 cells were treated with urea lysis buffer (6 mol/l urea, 2 mol/l thiourea, 3% CHAPS, 1% Triton X-100), and total cell lysate was recovered after centrifugation. Next, 100 μg of protein was separated using two-dimensional gel electrophoresis as described above, and target protein spots were recovered as gel plugs by using a protein spot recover machine (Molecular Hunter, AsOne, Osaka, Japan). Proteins in the gel plugs were manually digested using modified trypsin (Promega, Madison, WI, USA), and the trypsin digests were subjected to LC/MS (Finnigan LTQ linear ion trap mass spectrometer, Thermo Electron, San Jose, CA, USA). The Mascot search (version 2.1; Matrix Science, London, UK) was conducted to identify the mass of the peptide ion peaks compared with the SWISS PROT database (Homo sapiens, 12 867 sequences in the Sprot_47.8 FASTA file). Proteins with Mascot scores of ≥ 33 with at least 2 peptides were considered as positively identified.

Immunostaining and Confocal Microscopy

A total of 5×10^4 MDA-MB-231 cells were cultured on fibronectin-coated porous membrane for 2 days. The cells were washed 3 times with PBS and fixed with 4% formalin at room temperature for 15 min. Membranes were washed 3 times with PBS and permeabilized with 0.25% Triton-X (Sigma-Aldrich) in PBS at room temperature for 5 min. After washing 3 times with PBS, the membranes were incubated in blocking buffer containing 2% BSA in PBS for 10 min. The cells were treated with antibodies against RAB1A (1:12.5 dilution), TDRD7 (1:50 dilution), HSP90B (1:1000 dilution), and vimentin (1:100 dilution) (RV20, BD) in the blocking buffer for 2 h at room temperature. Subsequently, the cells were incubated with Alexa Flour 488–conjugated goat anti-rabbit IgG antibodies (1:100 dilution) (Molecular Probes, Invitrogen) against RAB1A, TDRD7, and HSP90B, and Alexa Flour 488–conjugated goat anti-mouse IgG antibody (Molecular Probes, Invitrogen, 1:100 dilution) against vimentin antibody in the blocking buffer for 1 h at RT. After washing 3 times with PBS, phalloidin (Sigma-Aldrich) staining was performed for 20 min at room temperature. Next, the stained cells on the membrane were washed 3 times with PBS, mounted, and covered with glass coverslips. The stained cells were then examined using a NIKON A1 confocal scanning system equipped with 488-nm argon and 568-nm helium-neon lasers (Nikon Corporation, Tokyo, Japan). X-Y-Z vertical sections were generated using a 0.5-μm motor step. Each image represents double averaged (40- to 50-line scan) images.

Construction of Plasmid Vectors Expressing RAB1A and siRNA against RAB1A

The cDNA construct for RAB1A inserts was amplified by PCR using KOD FX DNA polymerase (Toyobo, Osaka, Japan) with the following primer set: sense, 5′-CAGTGACA TGTCCAGCATGA-3′ (containing the first codon of RAB1A); antisense, 5′-GCAGCTACATACAGTACAATTCAGG-3′ (containing the stop codon of RAB1A). The PCR products were resolved by electrophoresis on 1% agarose gels and stained with ethidium bromide. Targeted bands were excised from gels and DNA was extracted and purified using the Wizard® SV Gel and PCR Clean-Up System (Promega) as described by the manufacturer. Extracted DNA was incubated at 70 °C with Taq polymerase and adenosine triphosphate for 30 min and ligated into pTA2 vector (Toyobo). Then, pTA2-RAB1A was enzymatically restricted with *Bam*HI and *Eco*RV. The

restricted pTA2-RAB1A was resolved by electrophoresis on 1% agarose gels and stained with ethidium bromide. Targeted bands were excised from gels and DNA was extracted and purified using the Wizard SV Gel and PCR Clean-Up System. Extracted DNA chains were annealed and ligated into the *Bam*HI/*Hpa*I sites of pCX4-bsr, a modified pCXbsr retroviral vector[18] provided by Dr T Akagi (Osaka Bioscience Institute, Osaka, Japan), and sequenced. The plasmids were extracted and the accuracy of the constructs was confirmed by sequencing.

The pSilencer4.1-CMVneo siRNA plasmid vector (Ambion, Austin, TX, USA) was used to construct pSilencer4.1-CMVneo-si-RAB1A and pSilencer4.1-CMVneo-scramble. A DNA chain with the RAB1A-targetting siRNA sequence or the scrambled fragment one was purchased from Ambion. The RAB1A-targetting sequences were as follows: 5′-GATCCCA ATCACCTCCAGTTATTATTCAAGAGATAATAACTGGAGGT GATTGTT-3′ (sense) and 5′-AGCTTAACAATCACCTCCAGT TATTATCTCTTGAATAATAACTGGAGGTGATTGG-3′ (antisense). The sequences had no homology with any other predicted protein-coding genes of the human genome according to manufacturer's instruction. The DNA chains were annealed and ligated into the *Bam*HI/*Hin*dIII sites of pSilencer4.1-CMVneo to generate pSilencer4.1-CMVneo-si-RAB1A. The negative control pSilencer4.1-CMVneo-scramble vector was constructed in the same manner. The plasmids were extracted and the accuracy of the insert sequence was confirmed by sequencing.

Transfection and Measurement of the Pseudopodial Length

For overexpression experiments, MDA-MB-231 cells on fibronectin-coated 3 μm porous membrane with NIH3T3-conditioned medium were transiently transfected with pCX4-bsr-RAB1A using FuGENE® 6 (Roche Applied Science, Indianapolis, IN, USA). In brief, 2.0×10^5 cells were seeded on 60 mm culture dishes overnight until 50–80% confluence was reached. Serum-free medium (194 μl) and 6.0 μl of FuGENE 6 reagent were mixed in 1.5 ml tubes and incubated for 5 min at room temperature. Plasmid vectors (2.0 μg each) were added and the contents were mixed and incubated with transfection reagent and DNA complex for at least 15 min at room temperature. The transfection reagent and DNA complex were added dropwise to the cultured cells and incubated for 48 h. For knockdown experiments, MDA-MB-231 cells were transfected transiently with the pSilencer4.1-CMVneo-si-RAB1A and scramble-pSilencer4.1-CMVneo vector constructs using Nucleofector with solution V (Lonza, Basel, Switzerland).

Then, the cells were immunostained with phalloidin and applied to confocal microscopy.

Statistical Analysis

Data about the length of the pseudopodial microprocesses were analyzed using Student's *t*-test and box plot method. A *P*-value of ≤ 0.05 was regarded as significant.

RESULTS

Pseudopodial Microprocesses in Porous Membranes

MDA-MB-231 breast cancer cells were seeded onto 10 μm thick membranes with 1 or 3 μm pores. We found that membrane protrusions (eg, pseudopodia) were extended into the membrane pores from the ventral side of the cell body (Figure 1a). Protrusion diameters were <10 nm and 1 μm in 1-μm (Figure 1a, left) and 3-μm (Figure 1a, right) porous membranes, respectively. Protrusion lengths varied from 2 to 10 μm in both types of porous membranes (Figure 1). Formation of membrane protrusions did not occur in the absence of NIH3T3-conditioned medium, although it was detectable when cells were cultured on 8 μm porous membrane (data not shown). Highly invasive melanoma cells, B16-F10 cells, formed similar membrane protrusions in the same tissue culture conditions as MDA-MB-231; however, nontumorigenic cells such as NIH3T3 did not (data not shown).

Isolation of Pseudopodial Microprocesses

An excimer laser-assisted cell etching technique was used to remove cell bodies from the porous membrane. A schematic diagram of the laser ablation is illustrated in Figure 1b and the video image of the laser ablation process is available in Supplementary Video Data. The video image showed that the cell body was removed in a short period. After treatment with an excimer laser-assisted cell etching, the membrane protrusions were observed to be dot-like structures (Figure 1c). Vertical images showed that cell bodies were completely removed and pseudopodia structures remained intact by visual inspection (Figure 1d). We examined the contents of integrin $\alpha 2$ that had accumulated in epithelial cell pseudopodia.[19] Immunoblotting also revealed that integrin $\alpha 2$ was highly enriched in the pseudopodia fraction compared with the whole cell, regardless of pore diameter, and without degradations (Figure 1e). In addition, enriched localization of integrin $\alpha 2$ was observed in pseudopodia on confocal imaging (Supplementary Figure S1).

Proteins Enriched in Pseudopodial Microprocess Extract

We compared protein content in pseudopodial microprocess extract (PME) and whole-cell extract (WCE) using 2D-DIGE and an internal control sample (Figure 2a). Proteome data resulting from 2D-DIGE included 2508 protein spots (Figure 2b and Supplementary Figure S2a). Scatter plot analysis demonstrated that high reproducibility was observed by performing the experiment in triplicate; the intensity of at least 97.2% protein spots was scattered within twofold differences (Supplementary Figure S2b). When identical samples were independently separated 3 times, the standardized and averaged intensity of at least 97.2% protein spots scattered within a twofold difference (Supplementary Figure S2b). Thus, the protein spots that met the following criteria were subjected to mass spectrometric protein identification: spots for the 1 μm porous membrane group, a false